THESIS FOR THE DEGREE OF LICENTIATE OF ENGINEERING

in

Thermo and Fluid Dynamics

Implementation of a flexible fiber model in a general purpose CFD code

by

Jelena Andrić

Department of Applied Mechanics
CHALMERS UNIVERSITY OF TECHNOLOGY
Göteborg, Sweden, 2012

Implementation of a flexible fiber model in a general purpose CFD code

JELENA ANDRIĆ

THESIS FOR LICENTIATE OF ENGINEERING no. 2012:04
ISSN 1652-8565

Department of Applied Mechanics
Chalmers University of Technology
SE-412 96 Göteborg
Sweden
Telephone +46-(0)31-7721388

Printed at Chalmers Reproservice
Göteborg, Sweden, 2012

Implementation of a flexible fiber model in a general purpose CFD code

JELENA ANDRIĆ

jelena.andric@chalmers.se
Department of Applied Mechanics
Chalmers University of Technology

Abstract

This work is related to the process of making pulp mats for use in hygienic products. One part of that process is the transportation of flexible cellulose fibers suspended in flowing air. The fibers should be evenly distributed on the substrate, and it is thus of high importance to avoid the formation of fiber flocks during the transportation. The purpose of the present work is to implement a flexible fiber model in a general purpose Computational Fluid Dynamics (CFD) code, for detailed studies of fiber-fiber and fiber-flow interaction in real flow situations. The fibers are modeled as chains of cylindrical segments, and the translational and rotational degrees of freedom of each segment are taken into account. Each segment is tracked individually, using Lagrangian Particle Tracking (LPT), and the equations of fiber motion are derived from the conservation of momentum for each segment. The segment inertia is taken into account and the one-way coupling with the fluid phase is considered. The fiber integrity is ensured through connectivity forces acting between the adjacent fiber segments. The implemented model has been applied both with imposed flow fields, and in a flow field simultaneously predicted by the CFD solver. The results show that the fibers are transported by the flow and are deformed due to flow gradients. Further, a generic test case is described and used to validate the energy conservation and response time of the fiber model concept.
This work is the foundation for further improvements of the fiber model through the addition of bending and twisting forces, as well as the inclusion of interaction (e.g. collision) forces between individual fiber segments. These features, together with a two-way coupling with the flow, will lead to a more complete fiber model.

Keywords: flexible fiber, LPT, CFD, OpenFOAM

Acknowledgments

I would like to thank my supervisor Håkan Nilsson for his guidance and support. Co-supervisors Alf-Erik Almstedt and Srdjan Sasic are also acknowledged.
Thanks to Henrik Rusche, Wikki GmbH and Hrvoje Jasak, Wikki Ltd. and FSB Zagreb, for their help with OpenFOAM during the NUMAP-Foam Summer school in Zagreb.
Many thanks to Djordje S. Čantrak and Milan Lečić from the University of Belgrade for the very useful discussion we had.
Moreover, I very much thank Stefan Lindström from Linköping University for our useful discussions and his help during the project.
This project has been financially supported by Bo Rydin Foundation and SCA Hygiene Products AB, which is greatly acknowledged.

Nomenclature

Latin Symbols

d	diameter	[m]
l	length	[m]
r	radius	[m]
e	aspect ratio	[-]
m	mass	[kg]
$\boldsymbol{I}$	inertia tensor	[kg m^2]
$\dot{\boldsymbol{I}}$	inertia tensor time derivative	[kg m^2/s]
$\boldsymbol{r}$	position	[m]
$\dot{\boldsymbol{r}}$	velocity	[m/s]
$\ddot{\boldsymbol{r}}$	acceleration	[m/s^2]
$\boldsymbol{\omega}$	angular velocity	[1/s]
$\hat{\boldsymbol{z}}$	orientation vector	[-]
$\boldsymbol{F}^h$	hydrodynamic force	[N]
$\boldsymbol{F}^w$	body force	[N]
$\boldsymbol{g}$	gravitational acceleration	[m/s^2]
$\boldsymbol{X}^h$	connectivity force	[N]
$\boldsymbol{f}^h$	contact force	[N]
$\boldsymbol{T}^h$	hydrodynamic torque	[Nm]
$\boldsymbol{Y}^h$	bending and twisting torque	[Nm]
$\boldsymbol{\upsilon}$	fluid velocity	[m/s]
$\boldsymbol{\Omega}$	fluid angular velocity	[1/s]
$\dot{\boldsymbol{\gamma}}$	strain rate tensor	[1/s]
$\boldsymbol{A}^v$,$\boldsymbol{C}^v$,$\boldsymbol{H}^v$	hydrodynamic resistance tensors	[kg/s]
$\boldsymbol{A}^I$,$\boldsymbol{C}^I$,$\boldsymbol{H}^I$	hydrodynamic resistance tensors	[kg/s]
X^A,Y^A,X^C,Y^C,Y^H	hydrodynamic coefficients	[-]
C_D	drag coefficient	[-]
Re_s	segment Reynolds number	[-]
E_p	potential energy	[J]
E_{kt}	translational kinetic energy	[J]

E_{kr}	rotational kinetic energy	[J]
E_{tot}	total energy	[J]
$\boldsymbol{a}$,$\boldsymbol{b}$,$\boldsymbol{c}$	vectors	[-]
$\boldsymbol{P}$,$\boldsymbol{S}$,$\boldsymbol{T}$	second-order tensors	[-]
$\boldsymbol{A}$	matrix	[-]
T	oscillatory period	[s]

Greek Symbols

Δt	time step	[s]
$\boldsymbol{\delta}$	Kronecker delta tensor	[-]
$\boldsymbol{\epsilon}$	permutation tensor	[-]
$\boldsymbol{\rho}$	density	[kg/m^3]
$\boldsymbol{\eta}$	dynamic viscosity	[kg/m s]
θ	angle	[rad]

Subscripts

i, j	segment indexes
n	time step index

Contents

Chapter 1

Introduction

This work deals with the description and numerical implementation of a model of fibers suspended in viscous, flowing fluid. Each fiber is modeled as a chain of cylindrical segments that are tracked using Lagrangian Particle Tracking. The segments are subjected to forces that make them stay attached, and drag forces that move and deform the fiber. The model is implemented in the OpenFOAM, an open source CFD tool, and is coupled with the imposed flow fields and a flow field that is simultaneously predicted by the CFD solver. The model can thus be used in different applications where flexible fiber suspensions in complex flow play an important role.
The aim of this work is to apply the method in the absorbent hygiene product industry, in applications such as the dry forming process of pulp mats, where fibers are suspended in flowing air. Controlling the fiber behaviour and interaction in these processes is essential in order to achieve the desired spatial arrangements of fibers in the final product. The development and the break-up of fiber flocks are of particular interest. Since such phenomena occur at the scales of the fiber length, it is difficult to study them experimentally. A particle-level simulation technique, described in this work, is an alternative tool for studying the fiber flow.

1.1 Background and Previous Work

The dynamic behavior of particles suspended in fluid flow is important in many processes in modern technology. In many of those suspensions nonspherical particles are present. One example is flexible fibers as well as their clusters. When a fiber suspension is subjected to a flow field, the fibers may translate, rotate and deform. In the case of the production of fiber mats, these changes in the suspension microstruc-

ture affect the produced material macroscopic properties, such as elastic modulus, strength, thermal and electric conductivities. In pulp and paper processing, fiber dynamics during the sheet forming process is one of the most important factors that influence the sheet characteristics [1, 2, 3].

Some of the current understanding of flexible fiber dynamics has its origin in experimental observations. Forgacs et al. [4, 5] identified different regimes for fiber motion in shear flow. They observed that flexible fibers subjected to shear flow move in a coloid regime with or without entanglement. These studies show that the dynamics of flexible fibers depend on the fiber stiffness, length, and the flow properties such as shear rate and fluid viscosity.

Some numerical approaches have been developed to study flows with particles. In the Eulerian-Eulerian approach, both the particle phase and the fluid phase are treated as a continuum. The Lagrangian-Eulerian approach treats particles as moving points in the fluid medium. In the DNS approach, the particle geometries are resolved at different levels of detail. In the microhydrodynamics approach many particles are combined in multi-rigid-body systems [6, 7]. Several numerical methods, which are using the microhydrodynamics approach have been developed to simulate flexible fiber motion in shear and sedimentation flows. Yamamoto and Matsuoka [3] developed a particle-level simulation technique for simulating the dynamic behavior of rigid and flexible fibers in a flow field. They regarded a fiber as a number of spheres, lined up and bonded to each neighboring sphere. Ross and Klingenberg [1] proposed a model similar to that of Yamamoto and Matsuoka, except that they model a fiber as a chain of rigid prolate spheroids. These numerical studies, both applied for two-dimensional viscous shear flow, were in qualitative agreement with experimental results for isolated fiber motion, reproducing the rigid, springy and snake-like regimes of fiber motion [4, 5]. However, the coiled regime of motion and the entanglment are three-dimensional phenomena and cannot be studied using two-dimensional models. Schmid et al. [8] developed a particle-level simulation technique to study the flocculation of fibers in sheared suspensions in three dimensions. They investigated the influence of shear rate, fiber shape and flexibility, and frictional interparticle forces on the flocculation phenomena. The fibers were modeled as chains of massless, rigid, cylindrical segments interacting with an imposed flow field through viscous drag forces and with other fibers through contact forces. The model did not account for particle inertia, hydrodynamic interactions or the two-way coupling between the fibers and the flow. Lindström and Uesaka [7] developed further the model

of Schmid et al. in an attempt to deal with the full complexity of fiber suspensions. The improved model accounts for the particle inertia and the hydrodynamic interaction between the fibers. They derived the approximation of the noncreeping interaction between fiber segment and the surrounding fluid, for larger segment Reynolds numbers, and took into account the two-way coupling. Their simulations successfully reproduced the different regimes of motion for threadlike particles ranging from rigid fiber motion to complicated orbiting behavior, including coiling with and without self-entanglement.

1.2 Aim and Limitations of the Present Work

This work is a first step towards the implementation of the model for flexible fibers in viscous fluid flow originally proposed by Schmid et al. [8] and further developed by Lindström and Uesaka [7] in the OpenFOAM, open source CFD software. The aim is to be able to obtain a detailed resolution of the flow field of the carrier phase, which is the main justification for the choice of software. The connectivity forces between adjacent fiber segments that ensure the integrity of a fiber are taken into account. The bending and twisting torques are currently not taken into account. The inter-segment interactions (e.g.collisions) and the segment-wall interactions are not considered. The implemented model is tested in different imposed flow fields as well as in the flow field obtained while simultaneously predicting the 2D transient laminar flow in a lid-driven cavity test case- a standard OpenFOAM tutorial with flow features that are relevant for the present application. In all the cases the one-way coupling is considered, i.e. the air flow is not affected by the presence of the fibers in the simulations. Furher, the energy conservation and response time of the fiber model concept is validated using a generic test case, resembling a physical pendulum.

1.3 Outline of the Thesis

Here, a short summary of the chapters and appendices is provided. Chapter 2 provides a theoretical background of this work. The fiber model geometry and the governing equations are presented. The limitations of the current implementation are pointed out as well. Chapter 3 summarizes the main results at the current stage of the work, considering both the imposed and the simultaneously predicted flow fields. Chapter 4 describes a generic test case, resembling a physical pendu-

lum, for validation of the energy conservation and response time of the fiber model concept. Appendix A is a short summary of the main vector and tensor operators that have been used in the derivation of a set of governing equations of motion for the fibers. Appendix B contains the derivation of the inertia tensor for a cylinder. Appendix C gives an overview of different numerical issues related to the model implementation, such as dimensional analysis and scaling, ill-conditioned linear systems and Tikhonov regularization. In Appendix D the complete derivation of the dimensionless fiber equations is shown. Appendix E describes the physical pendulum, which is used in Chapter 4 for validation purposes.

Chapter 2

Methodology

In this chapter a fiber geometry is first described, based on the concept of a chain of cylindrical segments. The dimensionless governing equations are presented, including the forces that have been taken into account in the current implementation. The numerical algorithms to solve these equations in order to get the unknown connectivity forces are also discussed.

2.1 Fiber Geometry

A fiber is in the present work modeled as a chain of N rigid cylindrical segments [7, 8], see Fig. 2.1. The segments are indexed $i \in [1, N]$ and their locations are specified with respect to a global Cartesian coordinate system Γ. The axes of the global cooordinate system are defined by the base vectors $\{\boldsymbol{x}_1, \boldsymbol{x}_2, \boldsymbol{x}_3\}$ and its origin is denoted by O. A single fiber segment has a diameter d_i, a length l_i, a start point P_i, a unit vector $\hat{\boldsymbol{z}}_i$, which is aligned with the segment, and another unit direction vector $\hat{\boldsymbol{y}}_i$, which is perpendicular to $\hat{\boldsymbol{z}}_i$. A local right-hand coordinate system Γ_i is associated with each fiber segment. The axes of a local coordinate system are defined by the orthonormal set $\hat{\boldsymbol{x}}_i, \hat{\boldsymbol{y}}_i, \hat{\boldsymbol{z}}_i$ and its origin is P_i, which is the start point of segment i. The diameter and length may differ between segments of the same fiber. For each fiber segment the position vector $\boldsymbol{r}_i = \overrightarrow{OP_i} + l_i\hat{\boldsymbol{z}}_i/2$ points out the fiber segment center of mass. The fiber segments rotate and twist about the joints, replicating the fiber bending and twisting deformations, while the fiber length remains constant. The bending and twisting torques attempt to hold the fiber in a specified equilibrium shape.

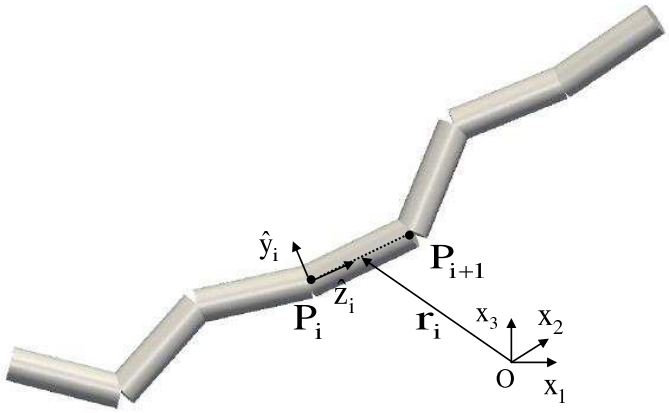

Figure 2.1: Fiber geometry definitions.

2.2 Equations of Motion

The equations of motion of a fiber represent the direct application of Newton's second law for each fiber segment i [7, 8]. The rate of change of linear momentum of fiber segment i is the sum of all forces that act on the segment, i.e.

$$m_i \ddot{\boldsymbol{r}}_i = \boldsymbol{F}_i^h + \boldsymbol{F}_i^w + \boldsymbol{X}_{i+1} - \boldsymbol{X}_i \tag{2.1}$$

Here m_i is the mass of the segment, $\boldsymbol{F}_i^h$ is the hydrodynamic force acting on the segment (see section 2.3), $\boldsymbol{F}_i^w$ is the sum of body forces, neglected in the present work except for the validation in Chapter 4 and $\boldsymbol{X}_i$ is the connectivity force exerted on segment $i-1$ by segment i. For the end segments $\boldsymbol{X}_1 = \boldsymbol{X}_{N+1} = \boldsymbol{0}$.
The rate of change of angular momentum about the center of gravity of the segment equals the moment of the external forces about that point, i.e.

$$\frac{\partial(\boldsymbol{I}_i \cdot \boldsymbol{\omega}_i)}{\partial t} = \boldsymbol{T}_i^h + \frac{l_i}{2}\hat{\boldsymbol{z}}_i \times \boldsymbol{X}_{i+1} + \left(\frac{-l_i}{2}\hat{\boldsymbol{z}}_i\right) \times (-\boldsymbol{X}_i) \tag{2.2}$$

where $\boldsymbol{I}_i$ is the tensor of inertia of segment i with respect to the global coordinate system Γ, $\boldsymbol{\omega}_i$ is is the angular velocity, $\boldsymbol{T}_i^h$ is the hydrodynamic torque. The connectivity constraints between fiber segments require that the end-points of adjacent fiber segments coincide, i.e.

$$\boldsymbol{r}_i + \frac{l_i}{2}\hat{\boldsymbol{z}}_i = \boldsymbol{r}_{i+1} - \frac{l_{i+1}}{2}\hat{\boldsymbol{z}}_{i+1} \tag{2.3}$$

The connectivity equation is then obtained by taking the time derivative of Eq. 2.3, i.e.

$$\dot{\boldsymbol{r}}_i - \dot{\boldsymbol{r}}_{i+1} = \frac{l_i}{2}\boldsymbol{\omega}_i \times \hat{\boldsymbol{z}}_i + \frac{l_{i+1}}{2}\boldsymbol{\omega}_{i+1} \times \hat{\boldsymbol{z}}_{i+1} \tag{2.4}$$

2.3 Hydrodynamic Forces

The hydrodynamic forces are taken into account in the equations as $\boldsymbol{F}_i^h$ and $\boldsymbol{T}_i^h$. The segment Reynolds number is defined as $Re_{s,i} = \rho d_i(\boldsymbol{v}(\boldsymbol{r}_i) - \dot{\boldsymbol{r}}_i)/\eta$, where d_i and $\dot{\boldsymbol{r}}_i$ are segment diameter and velocity, $\boldsymbol{v}(\boldsymbol{r}_i)$ is the fluid velocity at the segment center of gravity, and ρ and η are fluid density and dynamic viscosity respectively. The hydrodynamic forces are dominated by viscous effects for small segment Reynolds numbers, and by inertia effects for large segment Reynolds numbers. It can be assumed that the respective effects can be expressed as a sum of two separable components. Lindström and Uesaka [7] numerically investigated the consequence of this assumption, and found a good agreement between the model, theory and experiments in the viscous flow regime ($Re_s \lesssim 10^{-1}$) as well as in the regime dominated by dynamic effects ($10^2 \lesssim Re_s \gtrsim 3 \times 10^5$), while the highest discrepancy in drag coefficient C_D occured in the intermediate region and had a maximum of 42% at $Re_s \approx 5.4$. The total force and torque exerted on fiber segment i by the fluid are then given by

$$\boldsymbol{F}_i^h = (\boldsymbol{A}_i^v + \boldsymbol{A}_i^I) \cdot [\boldsymbol{v}(\boldsymbol{r}_i) - \dot{\boldsymbol{r}}_i] \tag{2.5}$$

$$\boldsymbol{T}_i^h = (\boldsymbol{C}_i^v + \boldsymbol{C}_i^I) \cdot [\boldsymbol{\Omega}(\boldsymbol{r}_i) - \boldsymbol{\omega}_i] + (\boldsymbol{H}_i^v + \boldsymbol{H}_i^I) : \dot{\boldsymbol{\gamma}}(\boldsymbol{r}_i) \tag{2.6}$$

Here $\boldsymbol{A}_i^v$, $\boldsymbol{C}_i^v$, and $\boldsymbol{H}_i^v$ are the hydrodynamic resistance tensors (see section 2.3.1) and $\boldsymbol{A}_i^I$, $\boldsymbol{C}_i^I$ and $\boldsymbol{H}_i^I$ are the dynamic drag resistance tensors (see section 2.3.2). $\boldsymbol{\Omega} = \nabla \times \boldsymbol{v}/2$ is the angular velocity of the fluid and $\dot{\gamma} = [\nabla \boldsymbol{v} + (\nabla \boldsymbol{v})^T]/2$ is the rate of strain tensor, where the gradient operator ∇ and the curl operator $\nabla\times$ are described in Appendix A. In the following sections, the approximations of the viscous and dynamic drag forces are described.

2.3.1 Viscous Drag Force

An analytical solution, described by Kim and Karilla [9], exists for the viscous drag force for isolated spheroidal particles and laminar conditions. According to the semi-empirical formula of Cox [10], a prolate spheroid is hydrodynamically equivalent to a finite circular cylinder in

the sense that their orbiting behavior in shear flow is the same if

$$\frac{r_e}{r_c} = 1.24\, ln(r_c)^{-1} \tag{2.7}$$

where r_e is a prolate spheroid equivalent aspect ratio and r_c is a cylinder aspect ratio. Since a fiber segment i is a cylinder of diameter d_i and lenght l_i its aspect ratio is $r_c = l_i/d_i$. The hydrodynamically equivalent prolate spheroid, whose major axis a_i equals a cylinder length l_i, has $r_e = l_i/b_i$, where b_i is a spheroid minor axis. From the Cox formula it follows that a cylindrical fiber segment i is hydrodynamically equivalent to a prolate spheroid whose minor axis b_i if

$$2b_i = \frac{1}{1.24} d_i \sqrt{ln\frac{l_i}{d_i}} \tag{2.8}$$

The Cox formula is valid for isolated particles and slender body approximation. None of these assumptions is true for fiber segments. However, Lindström and Uesaka [7] performed numerical experiments, which have shown that the error in the model predictions of orbit behavior for rigid fibers in shear flow becomes less than 3.4% compared to Eq.2.7 for $r_c \geq 10$ and when one-way coupling is considered. Thus, the viscous drag force of a fiber segment is here approximated with that of a prolate spheroid, in accordance to Kim and Karilla [9]. For a given velocity field $\boldsymbol{v}$ of the fluid, the viscous hydrodynamic force $\boldsymbol{F}_i^h$ and torque $\boldsymbol{T}_i^h$ are defined by

$$\boldsymbol{F}_i^{h,v} = \boldsymbol{A}_i^v \cdot [\boldsymbol{v}(\boldsymbol{r}_i) - \dot{\boldsymbol{r}}_i] \tag{2.9}$$

$$\boldsymbol{T}_i^{h,v} = \boldsymbol{C}_i^v \cdot [\boldsymbol{\Omega}(\boldsymbol{r}_i) - \boldsymbol{\omega}_i] + \boldsymbol{H}_i^v : \dot{\boldsymbol{\gamma}}(\boldsymbol{r}_i) \tag{2.10}$$

The hydrodynamic resistance tensors $\boldsymbol{A}_i^v$, $\boldsymbol{C}_i^v$ and $\boldsymbol{H}_i^v$ are defined as

$$\boldsymbol{A}_i^v = 3\pi\eta l_i [Y_i^A \boldsymbol{\delta} + (X_i^A - Y_i^A)\hat{\boldsymbol{z}}_i\hat{\boldsymbol{z}}_i] \tag{2.11}$$

$$\boldsymbol{C}_i^v = \pi\eta l_i^3 [Y_i^C \boldsymbol{\delta} + (X_i^C - Y_i^C)\hat{\boldsymbol{z}}_i\hat{\boldsymbol{z}}_i] \tag{2.12}$$

$$\boldsymbol{H}_i^v = -\pi\eta l_i^3 Y_i^H (\boldsymbol{\epsilon} \cdot \hat{\boldsymbol{z}}_i)\hat{\boldsymbol{z}}_i\hat{\boldsymbol{z}}_i] \tag{2.13}$$

where $\boldsymbol{\delta}$ and $\boldsymbol{\epsilon}$ are the unit and the permutation tensor, respectively and η is the fluid dynamic viscosity. The parameters X_i^A, Y_i^A, X_i^C, Y_i^C and Y_i^H are the hydrodynamic coefficients, which depend on the eccentricity

$e_i = (1 - b_i^2/a_i^2)^{1/2}$ and are defined as [9]

$$
\begin{aligned}
L(e_i) &= \ln \frac{1+e_i}{1-e_i} \\
X_i^A(e_i) &= \frac{8}{3} e_i^3 [-2e_i + (1+e_i^2) L(e_i)]^{-1} \\
Y_i^A(e_i) &= \frac{16}{3} e_i^3 [2e_i + (3e_i^2 - 1) L(e_i)]^{-1} \\
X_i^C(e_i) &= \frac{4}{3} e_i^3 (1-e_i^2) [2e_i - (1-e_i^2) L(e_i)]^{-1} \\
Y_i^C(e_i) &= \frac{4}{3} e_i^3 (2-e_i^2) [-2e_i - (1+e_i^2) L(e_i)]^{-1} \\
Y_i^H(e_i) &= \frac{4}{3} e_i^5 [-2e_i + (1+e_i^2) L(e_i)]^{-1}
\end{aligned}
\tag{2.14}
$$

2.3.2 Dynamic Drag Force

In this section the expressions for the dynamic drag force and torque on a cylindrical fiber segment at segment Reynolds number $10^2 \lesssim Re_s \lesssim 3 \times 10^5$ are presented. In this range of segment Reynolds numbers the drag force of cylinder in cross-flow is dominant compared to the viscous drag in the axial direction. If $\hat{\boldsymbol{z}}_i$ is the cylinder orientation, then only the flow components in the plane perpendicular to $\hat{\boldsymbol{z}}_i$ need to be considered. The drag coefficient for cross flow over a circular cylinder is $C_D^I = 1$, for $10^2 \lesssim Re_s \lesssim 3 \times 10^5$ [11]. The total drag force and torque on a cylindrical fiber segment are obtained through the integration over the infinitesimal cylinder slices. The dynamic drag force and torque are then given by

$$
\boldsymbol{F}_i^I \approx \boldsymbol{A}_i^I \cdot [\boldsymbol{v}(\boldsymbol{r}_i) - \dot{\boldsymbol{r}}_i] \tag{2.15}
$$

$$
\boldsymbol{T}_i^I \approx \boldsymbol{C}_i^I \cdot [\boldsymbol{\Omega}(\boldsymbol{r}_i) - \boldsymbol{\omega}_i] + \boldsymbol{H}_i^I : \dot{\boldsymbol{\gamma}}(\boldsymbol{r}_i) \tag{2.16}
$$

where the dynamic drag resistance tensors are

$$
\begin{aligned}
\boldsymbol{A}_i^I &= \frac{1}{2} C_D^I \rho d_i l_i v_{\perp,i}^* [\boldsymbol{\delta} - \hat{\boldsymbol{z}}_i \hat{\boldsymbol{z}}_i] \\
\boldsymbol{C}_i^I &= \frac{1}{24} C_D^I \rho d_i l_i^3 v_{\perp,i}^* [\boldsymbol{\delta} - \hat{\boldsymbol{z}}_i \hat{\boldsymbol{z}}_i] \\
\boldsymbol{H}_i^I &= \frac{1}{24} C_D^I \rho d_i l_i^3 v_{\perp,i}^* [(\boldsymbol{\epsilon} \cdot \hat{\boldsymbol{z}}_i)\, \hat{\boldsymbol{z}}_i]
\end{aligned}
\tag{2.17}
$$

and $v_{\perp,i}^*$ is the cross-flow velocity of the fluid relative to the fiber segment. The relative cross-flow velocity is given by $v_{\perp,i}^* = |\,(\boldsymbol{\delta} - \hat{\boldsymbol{z}}_i \hat{\boldsymbol{z}}_i) \times [\boldsymbol{v}(\boldsymbol{r}_i) - \dot{\boldsymbol{r}}_i]|$.

2.4 Discretization of Governing Equations

This section describes the discretization in time of the governing equations, starting with the linear momentum equation. The time step of the discretization is Δt. The subscripts $n-1$ and n stand for the values from the previous and the current time step respectively. An implicit numerical scheme is used while calculating the segment velocity and angular velocity, since it improves numerical stability. In all the equations that are presented in this section, the connectivity forces $\boldsymbol{X}_i$ and $\boldsymbol{X}_{i+1}$ are treated as unknowns. Using the expression for the hydrodynamic force (see section 2.3) and assuming $\boldsymbol{F}_i^w = 0$, Eq. 2.1 can be discretized as

$$\frac{m}{\Delta t}(\dot{\boldsymbol{r}}_{i,n} - \dot{\boldsymbol{r}}_{i,n-1}) = \left(\boldsymbol{A}_{i,n-1}^v + \boldsymbol{A}_{i,n-1}^I\right) \cdot \left[\boldsymbol{v}\left(\boldsymbol{r}_{i,n-1}\right) - \dot{\boldsymbol{r}}_{i,n}\right] + \boldsymbol{X}_{i+1,n} - \boldsymbol{X}_{i,n} \tag{2.18}$$

In the angular momentum equation the time differential term can be discretized as

$$\begin{aligned}\frac{\partial(\boldsymbol{I}_{i,n-1} \cdot \boldsymbol{\omega}_{i,n})}{\partial t} &= \dot{\boldsymbol{I}}_{i,n-1} \cdot \boldsymbol{\omega}_{i,n} + \boldsymbol{I}_{i,n-1} \cdot \dot{\boldsymbol{\omega}}_{i,n} \\ &\approx \dot{\boldsymbol{I}}_{i,n-1} \cdot \boldsymbol{\omega}_{i,n} + \frac{1}{\Delta t}\boldsymbol{I}_{i,n-1} \cdot (\boldsymbol{\omega}_{i,n} - \boldsymbol{\omega}_{i,n-1})\end{aligned} \tag{2.19}$$

Using the expression for the hydrodynamic force (see section 2.3), Eq. 2.2 can thus be discretized as

$$\begin{aligned}&\dot{\boldsymbol{I}}_{i,n-1} \cdot \boldsymbol{\omega}_{i,n} + \frac{1}{\Delta t}\boldsymbol{I}_{i,n-1} \cdot (\boldsymbol{\omega}_{i,n} - \boldsymbol{\omega}_{i,n-1}) = (\boldsymbol{C}_{i,n-1}^v + \boldsymbol{C}_{i,n-1}^I)\cdot \\ &(\boldsymbol{\Omega}\left(\boldsymbol{r}_{i,n-1}\right) - \boldsymbol{\omega}_{i,n}) + (\boldsymbol{H}_{i,n-1}^v + \boldsymbol{H}_{i,n-1}^I) : \dot{\boldsymbol{\gamma}}\left(\boldsymbol{r}_{i,n-1}\right) \\ &+ \frac{l_i}{2}\hat{\boldsymbol{z}}_{i,n-1} \times (\boldsymbol{X}_{i+1,n} + \boldsymbol{X}_{i,n})\end{aligned} \tag{2.20}$$

Finally, Eq. 2.4 is discretized as

$$\dot{\boldsymbol{r}}_{i,n} - \dot{\boldsymbol{r}}_{i+1,n} = \frac{l_i}{2}\boldsymbol{\omega}_{i,n} \times \hat{\boldsymbol{z}}_{i,n-1} + \frac{l_{i+1}}{2}\boldsymbol{\omega}_{i+1,n} \times \hat{\boldsymbol{z}}_{i+1,n-1} \tag{2.21}$$

The momentum equation, Eq. 2.18, the angular momentum equation, Eq. 2.20 and the connectivity equation, Eq. 2.21 form the system of equations, which can be solved for the unknown connectivity forces, velocities and angular velocities at time n. The numerical issues related to solving this system and the necessity to deal with a dimensionless set of equations is disussed in the next section.

2.4.1 Dimensionless Equations

In the governing equations shown in section 2.4, the velocities, angular velocities and connectivity forces are all treated as unknown. These variables have different physical units and therefore different orders of magnitudes. This will reflect in the coefficients of the linear system, which may differ by many orders of magnitude and make the system ill-conditioned. More details on ill-conditioned systems are given in Appendix C. One possible way to avoid this problem is to consider a dimensionless system of equations. In this section a short summary of the dimensionless equations is presented, while the complete derivation is shown in Appendix D. It is assumed that all fiber segments have the same diameter d and length l. The corresponding dimensionless hydrodynamic resistance tensors and dynamic drag resistance tensors at time $n-1$ are given by

$$
\begin{aligned}
\boldsymbol{A}^{\upsilon *}_{i,n-1} &= [Y^A \boldsymbol{\delta} + (X^A - Y^A)\hat{\boldsymbol{z}}_{i,n-1}\hat{\boldsymbol{z}}_{i,n-1}] \\
\boldsymbol{C}^{\upsilon *}_{i,n-1} &= [Y^A \boldsymbol{\delta} + (X^A - Y^A)\hat{\boldsymbol{z}}_{i,n-1}\hat{\boldsymbol{z}}_{i,n-1}] \\
\boldsymbol{H}^{\upsilon *}_{i,n-1} &= -Y^H \left(\boldsymbol{\epsilon} \cdot \hat{\boldsymbol{z}}_{i,n-1}\right) \hat{\boldsymbol{z}}_{i,n-1} \\
\boldsymbol{A}^{I *}_{i,n-1} &= \frac{\frac{1}{2} C_D^I \rho d \upsilon^*_{\perp,i}}{3\pi\eta} [\boldsymbol{\delta} - \hat{\boldsymbol{z}}_{i,n-1}\hat{\boldsymbol{z}}_{i,n-1}] \\
\boldsymbol{C}^{I *}_{i,n-1} &= \frac{\frac{1}{24} C_D^I \rho d \upsilon^*_{\perp,i}}{\pi\eta\dot{\gamma}} [\boldsymbol{\delta} - \hat{\boldsymbol{z}}_{i,n-1}\hat{\boldsymbol{z}}_{i,n-1}] \\
\boldsymbol{H}^{I *}_{i,n-1} &= -\frac{\frac{1}{24} C_D^I \rho d \upsilon^*_{\perp,i}}{\pi\eta\dot{\gamma}} [\left(\boldsymbol{\epsilon} \cdot \hat{\boldsymbol{z}}_{i,n-1}\right) \hat{\boldsymbol{z}}_{i,n-1}]
\end{aligned}
$$

The dimensionless discretized momentum, angular momentum and connectivity equation then read

$$
\frac{m^*}{\Delta t^*}(\dot{\boldsymbol{r}}^*_{i,n} - \dot{\boldsymbol{r}}^*_{i,n-1}) = (\boldsymbol{A}^{\upsilon *}_{i,n-1} + \boldsymbol{A}^{I *}_{i,n-1}) \cdot [\boldsymbol{\upsilon}^*(\boldsymbol{r}^*_{i,n-1}) - \dot{\boldsymbol{r}}^*_{i,n}] + \boldsymbol{X}^*_{i+1,n} - \boldsymbol{X}^*_{i,n} \tag{2.22}
$$

$$
\begin{aligned}
&\left(\dot{\boldsymbol{I}}^*_{i,n-1} + \frac{1}{\Delta t^*}\boldsymbol{I}^*_{i,n-1} + \boldsymbol{C}^{\upsilon *}_{i,n-1} + \boldsymbol{C}^{I *}_{i,n-1}\right) \cdot \boldsymbol{\omega}^*_{i,n} = \frac{1}{\Delta t^*}\boldsymbol{I}^*_{i,n-1} \cdot \boldsymbol{\omega}^*_{i,n-1} \\
&+ \left(\boldsymbol{C}^{\upsilon *}_{i,n-1} + \boldsymbol{C}^{I *}_{i,n-1}\right) \cdot \boldsymbol{\Omega}^*\left(\boldsymbol{r}^*_{i,n-1}\right) + \left(\boldsymbol{H}^{\upsilon *}_{i,n-1} + \boldsymbol{H}^{I *}_{i,n-1}\right) : \dot{\boldsymbol{\gamma}}^*\left(\boldsymbol{r}^*_{i,n-1}\right) \\
&+ \frac{3}{4r_p}\hat{\boldsymbol{z}}_{i,n-1} \times \left(\boldsymbol{X}^*_{i+1,n} + \boldsymbol{X}^*_{i,n}\right)
\end{aligned} \tag{2.23}
$$

$$
\dot{\boldsymbol{r}}^*_{i,n} - \dot{\boldsymbol{r}}^*_{i+1,n} + r_p(\boldsymbol{\omega}^*_{i,n} \times \hat{\boldsymbol{z}}_{i,n-1} + \boldsymbol{\omega}^*_{i+1,n} \times \hat{\boldsymbol{z}}_{i+1,n-1}) = \boldsymbol{0} \tag{2.24}
$$

where $r_P = l/2r = l/d$ is a fiber segment aspect ratio and the superscript $*$ stands for the dimensionless quantities.

The expressions for dimensionless velocity and angular velocity can be obtained from Eqs. 2.22 and 2.23

$$\dot{\boldsymbol{r}}^*_{i,n} = \left(\frac{m^*}{\Delta t^*}\boldsymbol{\delta} + \boldsymbol{A}^{v*}_{i,n-1} + \boldsymbol{A}^{I*}_{i,n-1}\right)^{-1} \cdot \big(\frac{m^*}{\Delta t^*}\dot{\boldsymbol{r}}^*_{i,n-1} + (\boldsymbol{A}^{v*}_{i,n-1} + \boldsymbol{A}^{I*}_{i,n-1}) \cdot \boldsymbol{v}(\boldsymbol{r}^*_{i,n-1}) + \boldsymbol{X}^*_{i+1,n} - \boldsymbol{X}^*_{i,n}\big) \tag{2.25}$$

$$\boldsymbol{\omega}^*_{i,n} = \left(\dot{\boldsymbol{I}}^*_{i,n-1} + \frac{1}{\Delta t^*}\boldsymbol{I}^*_{i,n-1} + \boldsymbol{C}^{v*}_{i,n-1} + \boldsymbol{C}^{I*}_{i,n-1}\right)^{-1} \cdot \big(\frac{1}{\Delta t^*}\boldsymbol{I}^*_{i,n-1} \cdot \boldsymbol{\omega}^*_{i,n-1} + (\boldsymbol{C}^{v*}_{i,n-1} + \boldsymbol{C}^{I*}_{i,n-1}) \cdot \boldsymbol{\Omega}^*\left(\boldsymbol{r}^*_{i,n-1}\right) + \left(\boldsymbol{H}^{v*}_{i,n-1} + \boldsymbol{H}^{I*}_{i,n-1}\right) : \dot{\boldsymbol{\gamma}}^*\left(\boldsymbol{r}^*_{i,n-1}\right) + \frac{3}{4r_p}\boldsymbol{C}^*_{\boldsymbol{z}\,i,n-1} \cdot \left(\boldsymbol{X}^*_{i+1,n} + \boldsymbol{X}^*_{i,n}\right)\big) \tag{2.26}$$

2.4.2 Connectivity Force Linear System

Substituting Eqs. 2.25-2.26 into Eq. 2.24 gives the dimensionless system of vectorial equations

$$\boldsymbol{Q}^*_{i,n-1} \cdot \boldsymbol{X}^*_{i,n} + \boldsymbol{S}^*_{i,n-1} \cdot \boldsymbol{X}^*_{i+1,n} + \boldsymbol{T}^*_{i,n-1} \cdot \boldsymbol{X}^*_{i+2,n} = \boldsymbol{V}^*_{i,n-1} \tag{2.27}$$

where

$$\boldsymbol{Q}^*_{i,n-1} = -(\frac{m^*}{\Delta t^*}\boldsymbol{\delta} + \boldsymbol{A}^{v*}_{i,n-1} + \boldsymbol{A}^{I*}_{i,n-1})^{-1} + \frac{3}{4r_p}\boldsymbol{C}^*_{\boldsymbol{z}\,i,n-1}$$

$$\boldsymbol{S}^*_{i,n-1} = (\frac{m^*}{\Delta t^*}\boldsymbol{\delta} + \boldsymbol{A}^{v*}_{i,n-1} + \boldsymbol{A}^{I*}_{i,n-1})^{-1} + (\frac{m^*}{\Delta t^*}\boldsymbol{\delta} + \boldsymbol{A}^{v*}_{i+1,n-1} + \boldsymbol{A}^{I*}_{i+1,n-1})^{-1} + \frac{3}{4r_p}\boldsymbol{C}^*_{\boldsymbol{z}\,i,n-1} + \frac{3}{4r_p}\boldsymbol{C}^*_{\boldsymbol{z}\,i+1,n-1}$$

$$\boldsymbol{T}^*_{i,n-1} = -(\frac{m^*}{\Delta t^*}\boldsymbol{\delta} + \boldsymbol{A}^{v*}_{i+1,n-1} + \boldsymbol{A}^{I*}_{i+1,n-1})^{-1} + \frac{3}{4r_p}\boldsymbol{C}^*_{\boldsymbol{z}\,i+1,n-1}$$

$$\boldsymbol{V}^*_{i,n-1} = -(\boldsymbol{s}^*_{i,n-1} - \boldsymbol{s}^*_{i+1,n-1} + r_p(\boldsymbol{b}^*_{i,n-1} + \boldsymbol{b}^*_{i+1,n-1}))$$

$$\boldsymbol{s}^*_{i,n-1} = (\frac{m^*}{\Delta t^*}\boldsymbol{\delta} + \boldsymbol{A}^{v*}_{i,n-1} + \boldsymbol{A}^{I*}_{i,n-1})^{-1} \cdot \big(\frac{m^*}{\Delta t^*}\dot{\boldsymbol{r}}^*_{i,n-1} + (\boldsymbol{A}^{v*}_{i,n-1} + \boldsymbol{A}^{I*}_{i,n-1}) \cdot \boldsymbol{v}^*(\boldsymbol{r}_{i,n-1})\big)$$

$$\boldsymbol{b}^*_{i,n-1} = \big((\boldsymbol{I}^*_{i,n-1} + \frac{1}{\Delta t^*}\boldsymbol{I}^*_{i,n-1} + \boldsymbol{C}^{v*}_{i,n-1} + \boldsymbol{C}^{I*}_{i,n-1})^{-1} \cdot \big(\frac{1}{\Delta t}\boldsymbol{I}^*_{i,n-1} \cdot \boldsymbol{\omega}^*_{i,n-1} + (\boldsymbol{C}^{v*}_{i,n-1} + \boldsymbol{C}^{I*}_{i,n-1}) \cdot \boldsymbol{\Omega}^*(\boldsymbol{r}_{i,n-1}) + (\boldsymbol{H}^{v*}_{i,n-1} + \boldsymbol{H}^{I*}_{i,n-1}) : \dot{\boldsymbol{\gamma}}^*_{i,n-1}(\boldsymbol{r}_{i,n-1})\big) \times \hat{\boldsymbol{z}}_{i,n-1}$$

where $\boldsymbol{C}^*_{\boldsymbol{z}\,i,n-1}$ is a second-order tensor, which is a function of tensor $\left(\dot{\boldsymbol{I}}^*_{i,n-1} + \frac{1}{\Delta t^*}\boldsymbol{I}^*_{i,n-1} + \boldsymbol{C}^{v*}_{i,n-1} + \boldsymbol{C}^{I*}_{i,n-1}\right)^{-1}$ and the orientation vector $\hat{\boldsymbol{z}}_{i,n-1}$

and its components are shown in Appendix D. After applying Tikhonov regularization (see Appendix C) this system can be solved for the unknown dimensionless connectivity forces $\boldsymbol{X}^*_{i,n}$, $[2 \leq i \leq N]$, while $\boldsymbol{X}^*_{1,n} = \boldsymbol{X}^*_{N+1,n} = \mathbf{0}$. In the present work each fiber consists of $N = 7$ segments and the system has the form

$$\begin{bmatrix} \boldsymbol{S}^*_{1,n-1} & \boldsymbol{T}^*_{1,n-1} & \mathbf{0} & \mathbf{0} & \mathbf{0} & \mathbf{0} \\ \boldsymbol{Q}^*_{2,n-1} & \boldsymbol{S}^*_{2,n-1} & \boldsymbol{T}^*_{2,n-1} & \mathbf{0} & \mathbf{0} & \mathbf{0} \\ \mathbf{0} & \boldsymbol{Q}^*_{3,n-1} & \boldsymbol{S}^*_{3,n-1} & \boldsymbol{T}^*_{3,n-1} & \mathbf{0} & \mathbf{0} \\ \mathbf{0} & \mathbf{0} & \boldsymbol{Q}^*_{4,n-1} & \boldsymbol{S}^*_{4,n-1} & \boldsymbol{T}^*_{4,n-1} & \mathbf{0} \\ \mathbf{0} & \mathbf{0} & \mathbf{0} & \boldsymbol{Q}^*_{5,n-1} & \boldsymbol{S}^*_{5,n-1} & \boldsymbol{T}^*_{5,n-1} \\ \mathbf{0} & \mathbf{0} & \mathbf{0} & \mathbf{0} & \boldsymbol{Q}^*_{6,n-1} & \boldsymbol{S}^*_{6,n-1} \end{bmatrix} \cdot \begin{bmatrix} \boldsymbol{X}^*_{2,n} \\ \boldsymbol{X}^*_{3,n} \\ \boldsymbol{X}^*_{4,n} \\ \boldsymbol{X}^*_{5,n} \\ \boldsymbol{X}^*_{6,n} \\ \boldsymbol{X}^*_{7,n} \end{bmatrix} = \begin{bmatrix} \boldsymbol{V}^*_{2,n-1} \\ \boldsymbol{V}^*_{3,n-1} \\ \boldsymbol{V}^*_{4,n-1} \\ \boldsymbol{V}^*_{5,n-1} \\ \boldsymbol{V}^*_{6,n-1} \\ \boldsymbol{V}^*_{7,n-1} \end{bmatrix} \tag{2.28}$$

2.4.3 Segment Position and Orientation Update

By substituting the computed dimensionless forces into Eqs. 2.25-2.26, the dimensionless velocity and angular velocity for a segment i are obtained. The dimensional velocities will then simply be obtained by scaling with the factors reciprocal to those used to make them dimensionless, i.e.

$$\begin{aligned} \dot{\boldsymbol{r}}_{i,n} &= r\dot{\gamma}\dot{\boldsymbol{r}}^*_{i,n} \\ \boldsymbol{\omega}_{i,n} &= \dot{\gamma}\boldsymbol{\omega}^*_{i,n} \end{aligned} \tag{2.29}$$

Once the velocities have been calculated, the new positions and orientations can be found for all segments. The updated segment position is given by

$$\boldsymbol{r}_{i,n} = \boldsymbol{r}_{i,n-1} + \dot{\boldsymbol{r}}_{i,n}\Delta t \tag{2.30}$$

The updated segment orientation reads

$$\hat{\boldsymbol{z}}_{i,n} = \hat{\boldsymbol{z}}_{i,n-1} + \Delta t\left(\boldsymbol{\omega}_{i,n} \times \hat{\boldsymbol{z}}_{i,n-1}\right) \tag{2.31}$$

Subscripts $n-1$ and n once again stand for the values from the previous and the current time step respectively.

Chapter 3

Case Descriptions, Results and Discussion

The implemented fiber model has been tested in different types of flows. The simplest flows are imposed velocity distributions where only the fiber motion is simulated interpolating the required flow values from the imposed flow field. A more advanced flow is the lid-driven cavity case in two dimensions, where both the flow and fiber motion are solved for simultaneously. The case is based on one of the standard tutorial cases in OpenFOAM for simplicity. It has many of the flow features that the fibers will encounter in the real applications. In all the cases that are presented in this work the fluid is air, whose properties are density $\rho = 1.2$ kg/m^3 and kinematic viscosity $\nu = 1.5 \cdot 10^{-5}$ m^2/s. Regarding the fiber properties, each segment has diameter $d = 50$ μm, length $l = 1$ mm and density $\rho = 1380$ kg/m^3, which is the density of a cellulose fiber. The fibers are set in the computational domain and the initial positions and orientations an for all fiber segments for all fibers are assigned. The fibers can have horizontal, vertical or zig-zag shape. First, the simulation results for several different imposed flow fields are analyzed. Secondly, the results for the coupled simulation are analyzed.

3.1 Imposed Flow Fields

For the imposed flow fields, the computational domain is a box of side 0.1m, see Fig. 3.1(a). The domain is decomoposed into a Cartesian mesh with 10 cells in each direction. The number of cells is choosen to accurately resolve the imposed flow gradient, and to keep the fibers away from the boundary cells. Each case includes 50 fibers, but may be easily specified differently. The initial fiber positions and shapes are

shown in Fig. 3.1.

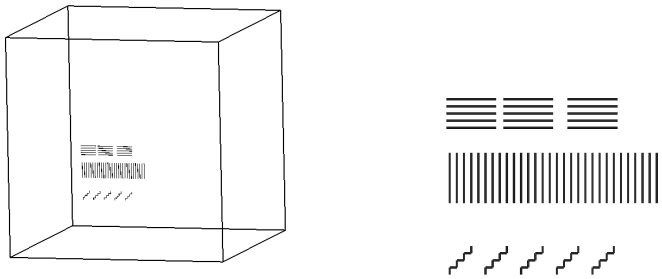

(a) Time = 0s; Positions in the box (b) Time = 0s; Shapes in a z plane

Figure 3.1: Computational domain with fibers at their initial positions and shapes, for the imposed flow studies.

3.1.1 Case $\boldsymbol{u} = (y, 0, 0)$

The imposed velocity profile is a simple shear $\boldsymbol{u} = (y, 0, 0)$. The shear rate is thus $\dot{\gamma} = 1$. Fig. 3.2 shows the result of the simulation. For the horizontal fibers it can be seen that the fibers having higher y position move faster, as they should. The vertical and zig-zag fibers respond to the flow by moving and rotating according to the flow direction and rotation. The fiber segments stay connected, but since the fiber model does not include bending and twisting, it is not possible to draw any further conclusion. However some observations can be pointed out. It can be seen that in the case of the zig-zag fibers, the whole fiber is deformed and it tends to stretch out in the flow direction. Thus, the fiber shape evolution depends on its initial shape. Including the bending force in the implementation would reduce this effect and keep the fiber more similar to its equilibrium shape.

3.1.2 Case $\boldsymbol{u} = (10y, 0, 0)$

In this test case the imposed flow field is again a simple shear flow, with $\boldsymbol{u} = (10y, 0, 0)$ and the shear rate is thus $\dot{\gamma} = 10$. Fig. 3.3 shows the result of the simulation. Conclusions similar to the previous test case can be made. The fibers respond faster to the flow, as expected, and reach the right end of the computational domain in approximately 0.1s. At this time the horizontal and vertical fibers have the same pattern as in case of shear rate $\dot{\gamma} = 1$, at time 1s. The zig-zag fibers do not completely align with the flow. It can be seen that the first segment is more bent with respect to the previous case.

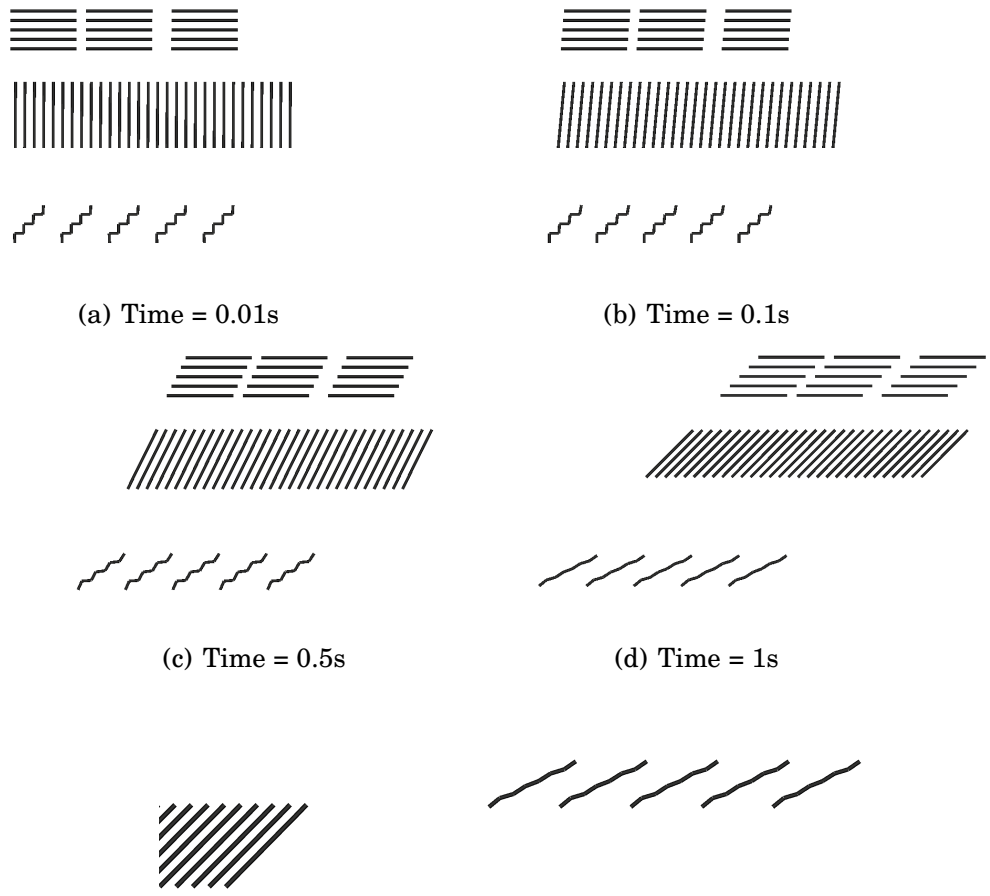

(a) Time = 0.01s (b) Time = 0.1s

(c) Time = 0.5s (d) Time = 1s

(e) Time = 1s; zoom-up at vertical fibers (f) Time = 1s; zoom-up at zig-zag fibers

Figure 3.2: Fibers in a simple shear flow $\boldsymbol{u} = (y, 0, 0)$.

3.1.3 Case $\boldsymbol{u} = (100y, 0, 0)$

The imposed simple shear is in this case $\boldsymbol{u} = (100y, 0, 0)$, with the shear rate $\dot{\gamma} = 100$. The fibers are in this case approaching the right end of the computational domain in 0.01s. The results are shown in Fig. 3.4 and it can be seen that the horizontal fibers have similar pattern as for cases $\boldsymbol{u} = (y, 0, 0)$ at time 1s, and $\boldsymbol{u} = (10y, 0, 0)$ at time 0.1s. In the case of initially vertical fibers it can be seen that the first and last segment are slightly bent with respect to the remaining fiber. Those segments experience only one connectivity force, since the forces at both ends are zero, while the inner segments feel the connectivity force from both sides. The balance between connectivity force and flow forces is causing the moment which causes those two segments to missalign with the rest of the fiber. For the zig-zag fibers the different shape compared to

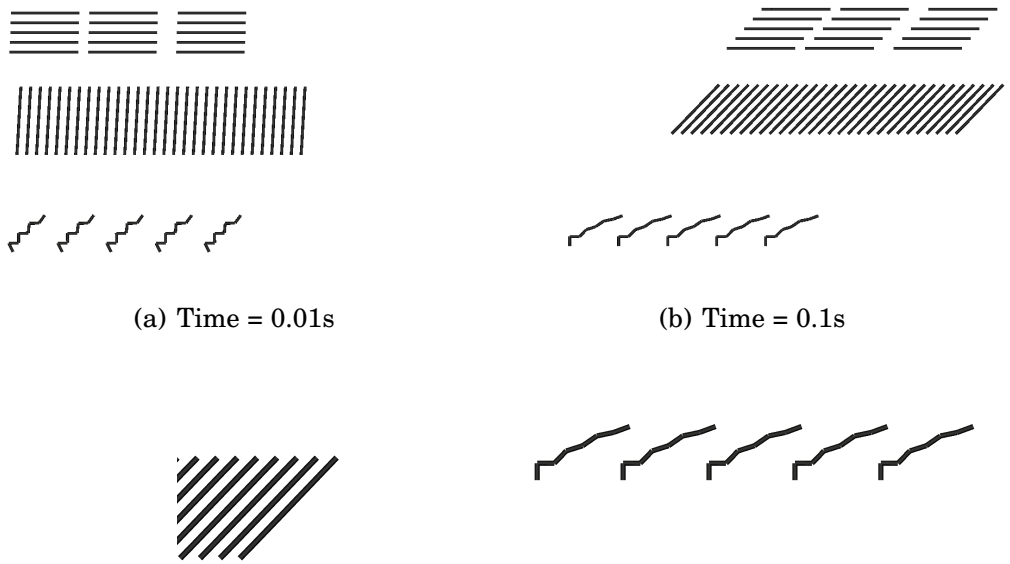

(a) Time = 0.01s

(b) Time = 0.1s

(c) Time = 0.1s; zoom-up at vertical fibers

(d) Time = 0.1s; zoom-up at zig-zag fibers

Figure 3.3: Fibers in a simple shear flow $\boldsymbol{u} = (10y, 0, 0)$.

the previous cases can be observed. The first segment of zig-zag fibers is more bent and it almost overlaps the second one. The rest of the fiber is deformed as well and does not align with the flow. The deformations seen for the vertical and zig-zag fibers are related to the segment Reynolds number, which in this case becomes higher than 1 and the inertial drag force becomes important. Thus, it can be concluded that the fiber shape evolution depends on the shear rate.

3.1.4 Case $\boldsymbol{u} = (0, x, 0)$

The imposed fluid flow field is in this case $\boldsymbol{u} = (0, x, 0)$. This is similar to case $\boldsymbol{u} = (y, 0, 0)$, but with the flow in the vertical direction. The results are shown in Fig. 3.5. The vertical fibers having higher x position move faster and remain straight. For the horizontal fibers the segments experiencing higher velocity move upwards and rotate. The zig-zag fibers stretch out in the flow direction as in the case $\boldsymbol{u} = (y, 0, 0)$.

3.1.5 Case $\boldsymbol{u} = (y, x, 0)$

The imposed fluid flow field is in this case $\boldsymbol{u} = (y, x, 0)$. This case is set up to test the model for a flow that has two non-zero components.

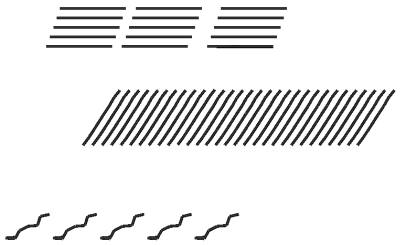

(a) Time = 0.01s

(b) Time = 0.01s; zoom-up at vertical fibers

(c) Time = 0.01s; zoom-up at zig-zag fibers

Figure 3.4: Fibers in a simple shear flow $\boldsymbol{u} = (100y, 0, 0)$.

From the results shown in Fig. 3.6 it can be seen that the fiber motion takes place in the xy plane, vertically upwards and to the right end of the domain, which is reached in 0.7s. The vertical and horizontal fibers keep their initial shape as in the cases $\boldsymbol{u} = (y, 0, 0)$ and $\boldsymbol{u} = (0, x, 0)$, while the zig-zag fibers are completely stretched out and follow the flow. Conclusions analogous to the previous cases apply here as well.

3.2 Simultaneously Predicted Flow Field

In order to show that the implemented fiber model can be coupled with a solver for the fluid phase, the standard 2D, transient and laminar lid-driven cavity OpenFOAM tutorial is used as an initial test case. The case and the results of the simulation are described in section 3.2.1.

3.2.1 Lid-Driven Cavity

The lid-driven cavity computational domain is a square with sides 0.1 m. All the boundaries of the square are walls. The top wall has a velocity of 0.1 m/s in the x direction, while the remaining three walls are stationary. The flow is assumed to be laminar and it is solved using a modified version of the original icoFoam solver in which calls to the fiber model have been added. The icoFoam solver is implemented for

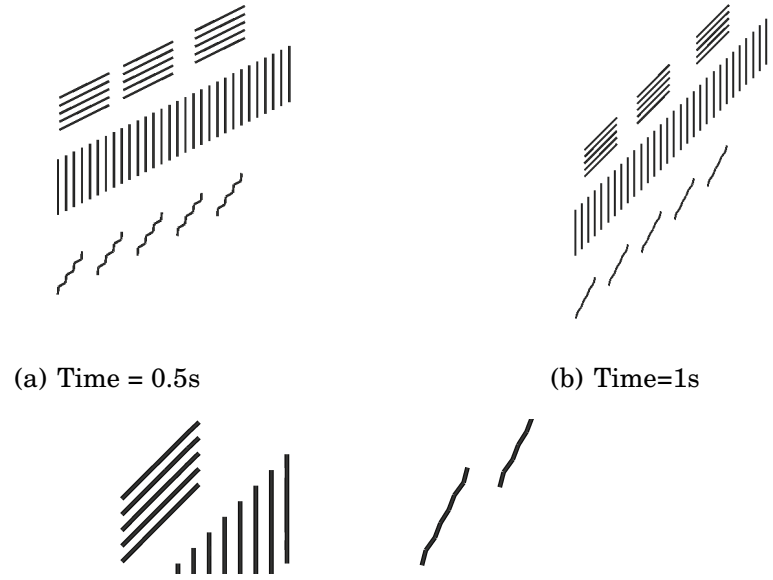

(a) Time = 0.5s (b) Time=1s

(c) Time = 1s; zoom-up at horizontal fibers (d) Time = 1s; zoom-up at zig-zag fibers

Figure 3.5: Fibers in a simple shear flow $\boldsymbol{u} = (0, x, 0)$.

laminar, isothermal, incompressible flow of Newtonian fluids. The flow is in the present case regarded as two-dimensional. It should be noted that the fiber model is always three-dimensional. A graded Cartesian mesh with 100 cells in both x and y directions is used for this case. The mesh is refined in the region close to the upper wall and to the right of the computational domain. The purpose of using a graded mesh is to avoid having fibers in the cell layers next to the top and right wall.
From the results shown in Figs. 3.7-3.10 it can be seen that the fibers move with the developing flow field and that the fiber segments stay connected. The zig-zag fibers straighten when following the flow, and both, the horizontal and the zig-zag fibers align with the flow field.

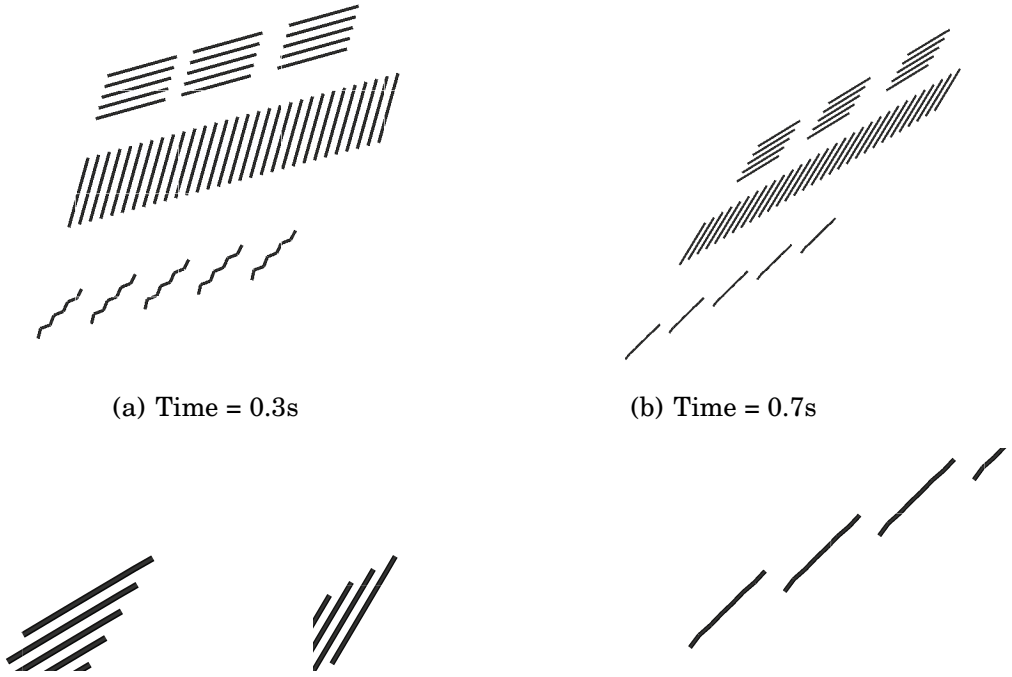

(a) Time = 0.3s

(b) Time = 0.7s

(c) Time = 0.7s; zoom-up at horizontal fibers

(d) Time = 0.7s; zoom-up at vertical fibers

(e) Time = 0.7s; zoom-up at zig-zag fibers

Figure 3.6: Fibers in a simple shear flow $\boldsymbol{u} = (y, x, 0)$.

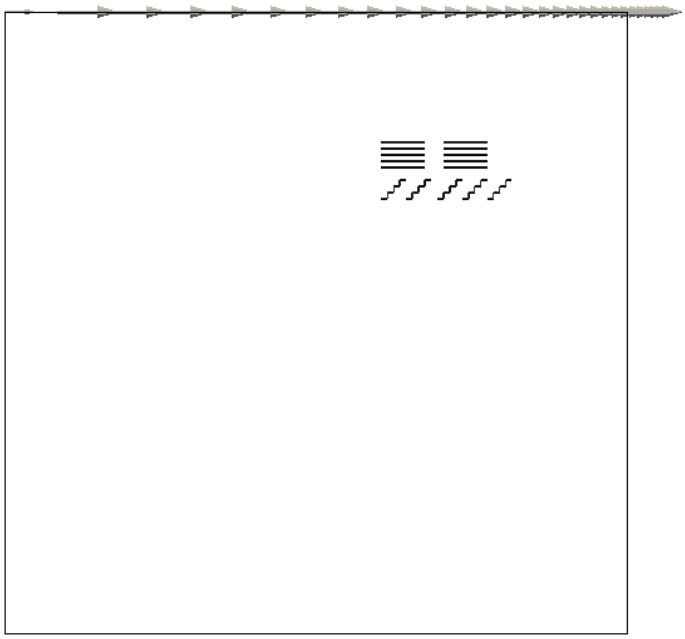

(a) Time = 0s

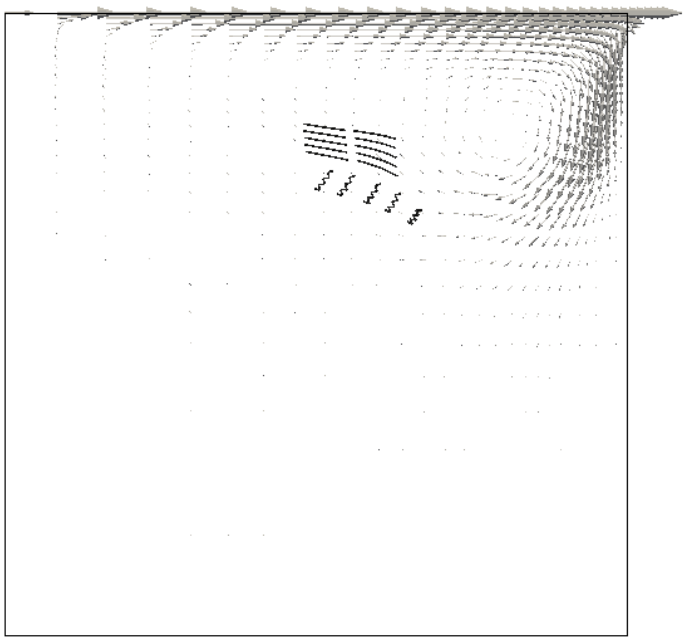

(b) Time = 2s

Figure 3.7: Fibers in cavity 2D flow

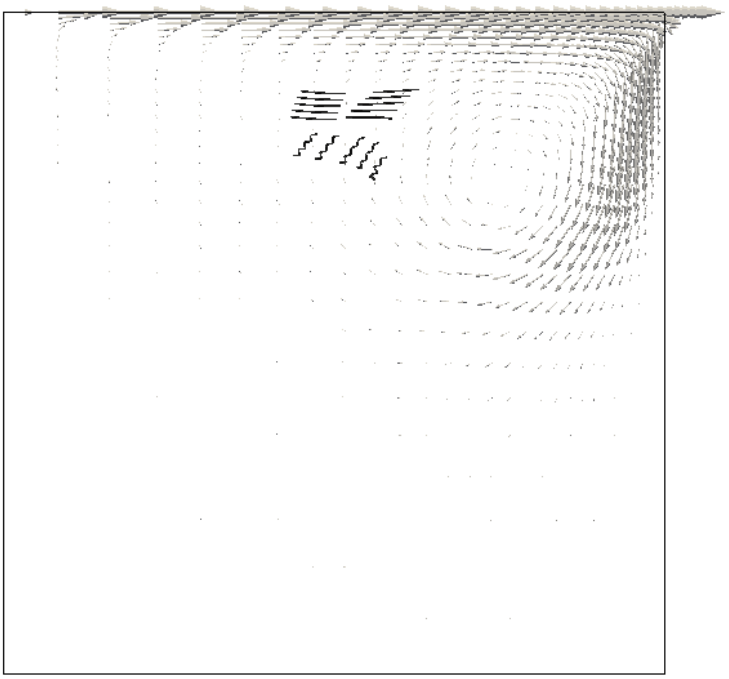

(a) Time = 3s

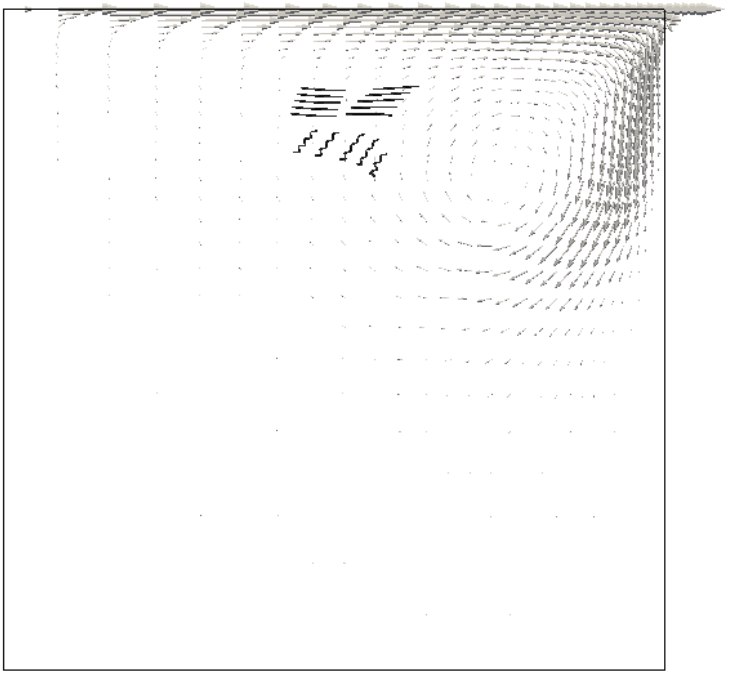

(b) Time = 4s

Figure 3.8: Fibers in cavity 2D flow.

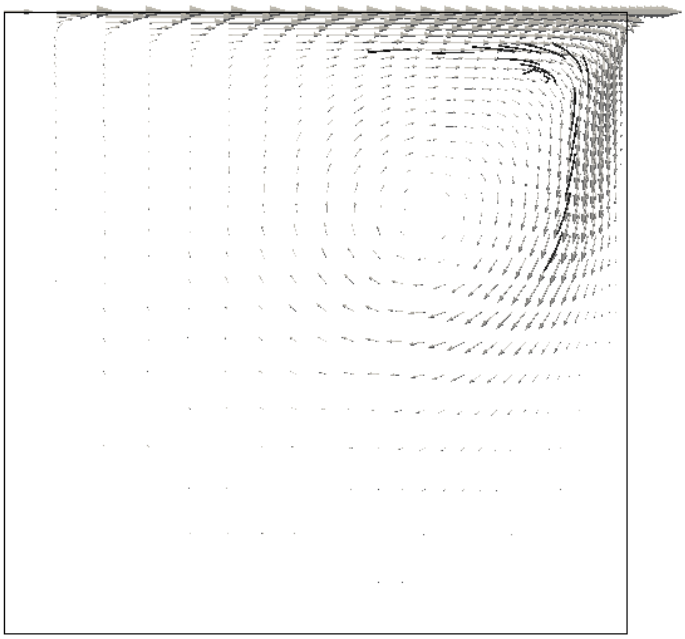

(a) Time = 5s

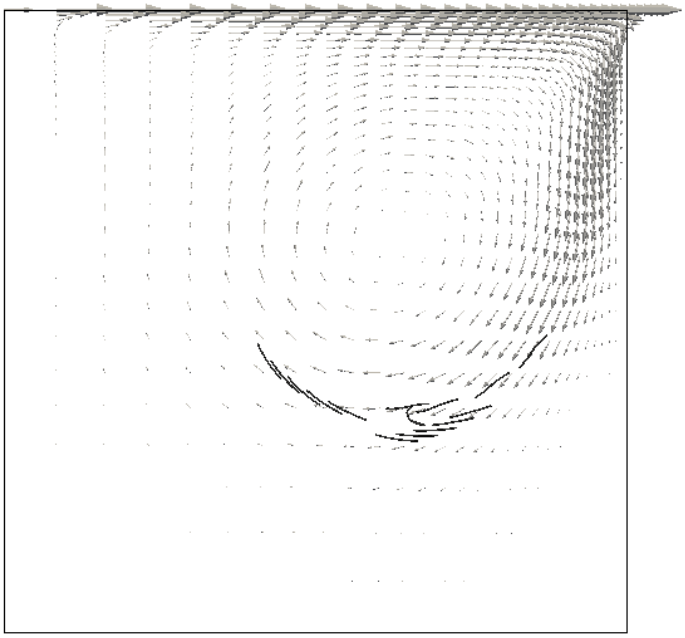

(b) Time = 7s

Figure 3.9: Fibers in cavity 2D flow.

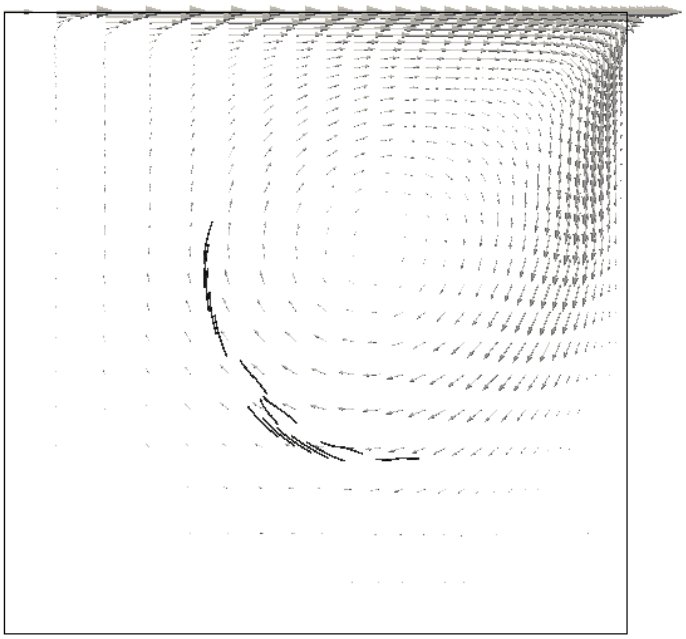

(a) Time = 8s

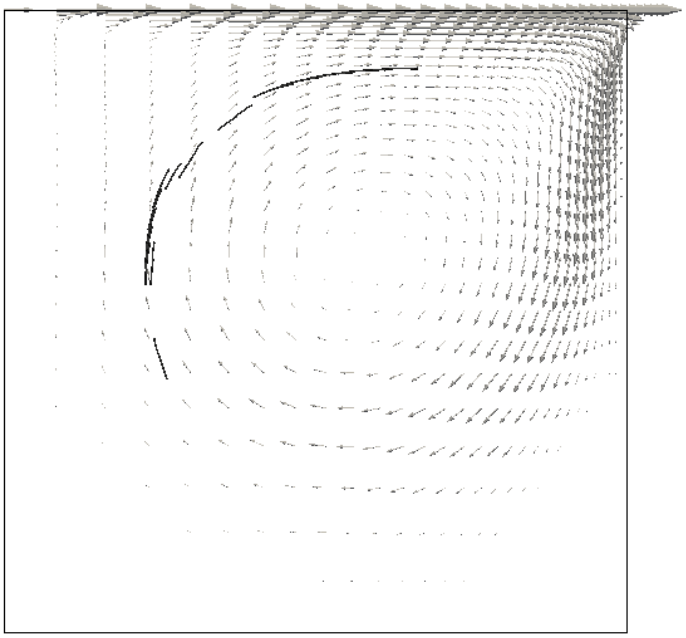

(b) Time = 10s

Figure 3.10: Fibers in cavity 2D flow.

Chapter 4

Validation of Energy Conservation and Response Time

4.1 Test Case Description

A simple mechanical system, consisting of two connected thin rods, having mass m and length l, is here considered. The rods are positioned in the xy plane, such that the end point of rod 1 coincides with the start point of rod 2. The position vectors for the centers of mass are $\boldsymbol{r}_1 = (-l/2\sin(\theta), l/2\cos(\theta), 0)$ and $\boldsymbol{r}_2 = (l/2\sin(\theta), -l/2\cos(\theta), 0)$. The orientation vectors are $\hat{\boldsymbol{z}}_1 = (\sin(\theta), -\cos(\theta), 0)$ and $\hat{\boldsymbol{z}}_2 = (\sin(\theta), -\cos(\theta), 0)$, where θ is the angle between the rod orientation axis and the $-y$ axis. The body forces $-\boldsymbol{F}^w$ and $\boldsymbol{F}^w$ are applied at the centers of mass of rod 1 and 2, respectively, where $\boldsymbol{F}^w = m\boldsymbol{g}$ and $\boldsymbol{g} = (0, -9.81, 0)$. The use of the acceleration $\boldsymbol{g}$ makes rod 1 resemble a physical pendulum, fixed at the pivot point O, under gravitational acceleration. Rod 2 is thus a mirrored version of rod 1, with the purpose of fixing the pivot point O through the forced connectivity. Rod 1 exerts the connectivity force $\boldsymbol{X}$ on rod 2, and consequently rod 2 exerts the connectivity force $-\boldsymbol{X}$ on rod 1. It should be noted that the present fiber model treats segment rotation about a point that is not coinciding with its center of gravity as a sum of rotation about the center of gravity and translation. It is therefore of interest to validate that this representation conserves the energy, and gives the same period as a physical pendulum motion about a pivot point.

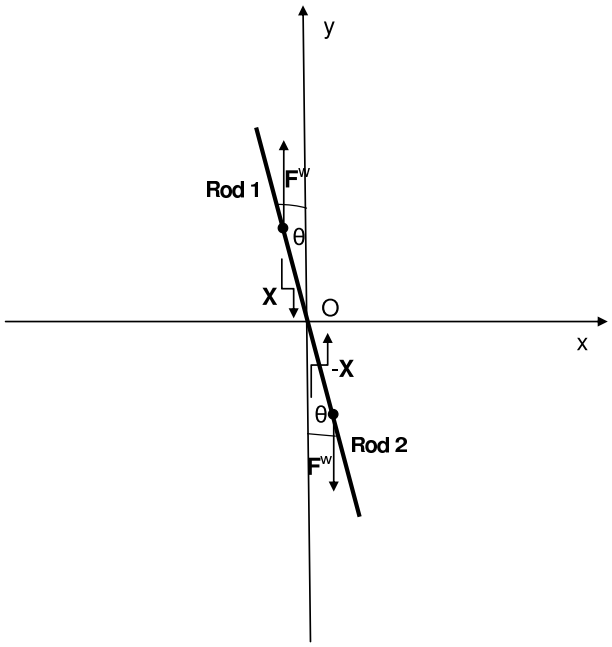

Figure 4.1: Two-rod mechanical system

4.2 Equations of Motion

The set of equations of motion for this mechanical system is a simplified version of the ones in Chapter 2. The flow interaction is here exchanged with a constant body force. The linear momentum equations are written as

$$m\ddot{\boldsymbol{r}}_1 = -\boldsymbol{F}^w + \boldsymbol{X} \tag{4.1}$$

$$m\ddot{\boldsymbol{r}}_2 = \boldsymbol{F}^w - \boldsymbol{X} \tag{4.2}$$

The motion of the rods is, according to the fiber model, decomposed into a rotation about the center of mass and a translation. The moment of inertia is thus given by $I = \frac{1}{12}ml^2$, i.e. is a scalar constant since the rods are considered infinitely thin. Thus, the angular momentum equations reduce to

$$I\dot{\boldsymbol{\omega}}_1 = \frac{l}{2}\hat{\boldsymbol{z}}_1 \times \boldsymbol{X} \tag{4.3}$$

$$I\dot{\boldsymbol{\omega}}_2 = \frac{l}{2}\hat{\boldsymbol{z}}_2 \times \boldsymbol{X} \tag{4.4}$$

The corresponding equations in the discretized form read

$$\dot{\boldsymbol{r}}_{1,n} = \dot{\boldsymbol{r}}_{1,n-1} + \Delta t \left(-\frac{\boldsymbol{F}^w}{m} + \frac{\boldsymbol{X}_n}{m} \right) \tag{4.5}$$

$$\dot{\boldsymbol{r}}_{2,n} = \dot{\boldsymbol{r}}_{2,n-1} + \Delta t \left(\frac{\boldsymbol{F}^w}{m} - \frac{\boldsymbol{X}_n}{m} \right) \tag{4.6}$$

$$\boldsymbol{\omega}_{1,n} = \boldsymbol{\omega}_{1,n-1} + \Delta t \left(\frac{l}{2I} \right) (\hat{\boldsymbol{z}}_{1,n-1} \times \boldsymbol{X}_n) \tag{4.7}$$

$$\boldsymbol{\omega}_{2,n} = \boldsymbol{\omega}_{2,n-1} + \Delta t \left(\frac{l}{2I} \right) (\hat{\boldsymbol{z}}_{2,n-1} \times \boldsymbol{X}_n) \tag{4.8}$$

The discretized connectivity equation is given by

$$\dot{\boldsymbol{r}}_{1,n} - \dot{\boldsymbol{r}}_{2,n} + \frac{l}{2} \left(\boldsymbol{\omega}_{1,n} \times \hat{\boldsymbol{z}}_{1,n-1} + \boldsymbol{\omega}_{2,n} \times \hat{\boldsymbol{z}}_{2,n-1} \right) = \boldsymbol{0} \tag{4.9}$$

The subscript $n-1$ stands for the values from the previous time step. Substituting Eqs. 4.5-4.8 into Eq. 4.9 gives the system

$$\boldsymbol{A}_{n-1} \cdot \boldsymbol{X}_n = \boldsymbol{b}_{n-1} \tag{4.10}$$

where

$$\boldsymbol{A}_{n-1} = \frac{2\Delta t}{m} \boldsymbol{\delta} + \frac{l^2}{4I} \Delta t \left(2\boldsymbol{\delta} - \hat{\boldsymbol{z}}_{1,n-1} \hat{\boldsymbol{z}}_{1,n-1} - \hat{\boldsymbol{z}}_{2,n-1} \hat{\boldsymbol{z}}_{2,n-1} \right)$$

$$\boldsymbol{b}_{n-1} = -\left(\dot{\boldsymbol{r}}_{1,n-1} - \dot{\boldsymbol{r}}_{2,n-1} - 2\frac{\boldsymbol{F}^w}{m} \Delta t + \frac{l}{2} \left(\boldsymbol{\omega}_{1,n-1} \times \hat{\boldsymbol{z}}_{1,n-1} + \boldsymbol{\omega}_{2,n-1} \times \hat{\boldsymbol{z}}_{2,n-1} \right) \right)$$

The connectivity force $\boldsymbol{X}_n$ is simply obtained by

$$\boldsymbol{X}_n = \boldsymbol{A}_{n-1}^{-1} \cdot \boldsymbol{b}_{n-1} \tag{4.11}$$

Substituting the value for the force $\boldsymbol{X}$ into the Eqs. 4.5-4.8 yields the translational and angular velocities, and consequently the updated rod positions and orientations.

4.3 Numerical Test

The motion of the system is here numerically analyzed. For simplicity, it is assumed that $m = 1$ kg and $l = 1$ m. Fig. 4.2 shows that the rods stay connected and that the connectivity point remains fixed during the pendulum motion. The whole sytem can be viewed as it oscillates around the point connecting the rods.

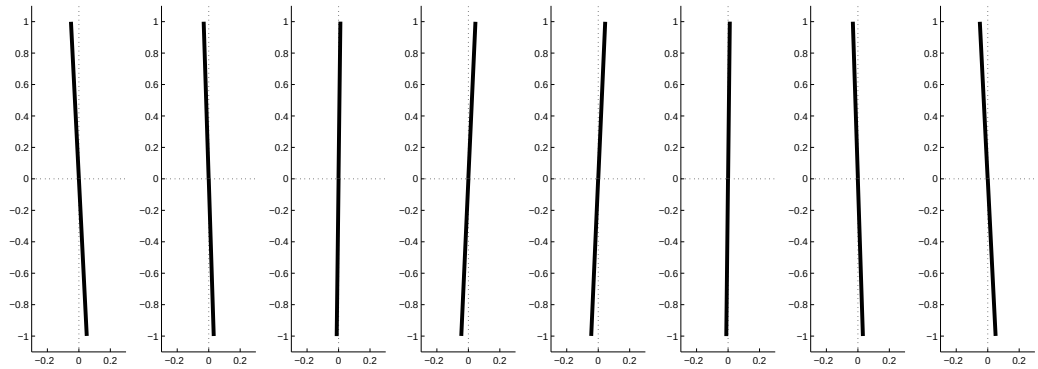

Figure 4.2: Two-rod system motion for different time steps; from left to right Time = 0s, 0.23s, 0.47s, 0.70s, 0.94s, 1.17s, 1.41s, 1.64s

4.4 Energy Conservation Concept

The total energy of each rod is the sum of the potential energy and the total kinetic energy. The total kinetic energy is the sum of translational kinetic energy E_{kt}, and the rotational kinetic energy E_{kr} around the center of gravity. The corresponding energies are thus for each rod given by

$$E_p = mg\frac{l}{2}\left(1 - cos\left(\theta\right)\right) \tag{4.12}$$

$$E_{kt} = \frac{1}{2}m\dot{\boldsymbol{r}}^2 \tag{4.13}$$

$$E_{kr} = \frac{1}{2}I\boldsymbol{\omega}^2 \tag{4.14}$$

The total kinetic energy of each rod is

$$E_{tot} = E_p + E_{kt} + E_{kr} \tag{4.15}$$

The potential, kinetic and total energy for each rod are shown in Fig. 4.3. It can be seen that the total energy is transformed between the potential and the kinetic energies and is conserved over time. The potential energy is highest while the rod is at its largest angle θ, and the lowest when it is aligned with the y axis. Vice versa for the kinetic energy. The oscillatory period of the mechanical system, obtained from the numerical test is $T_{numerical} = 1.64$ s and it compares well with the period of the analytical result for a pendulum, i.e. $T_{analytical} = 1.637$ s. The analytical expression is derived in Appendix E. A comparison beween the rod translational and rotational kinetic energy is shown in

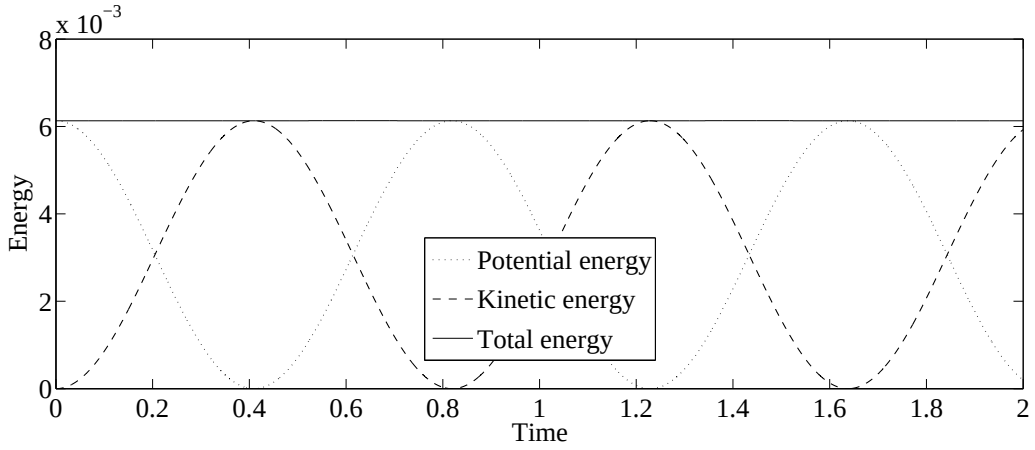

Figure 4.3: Total energy conservation over time

Fig. 4.4 and it can be seen that the greatest part of the kinetic energy comes from the translational motion. This is different to the real case of a physical pendulum with a moment of inertia about the pivot point, where all the kinetic energy is in the form of rotational energy. However, the present study verifies that the current concept yields the same pendulum motion.

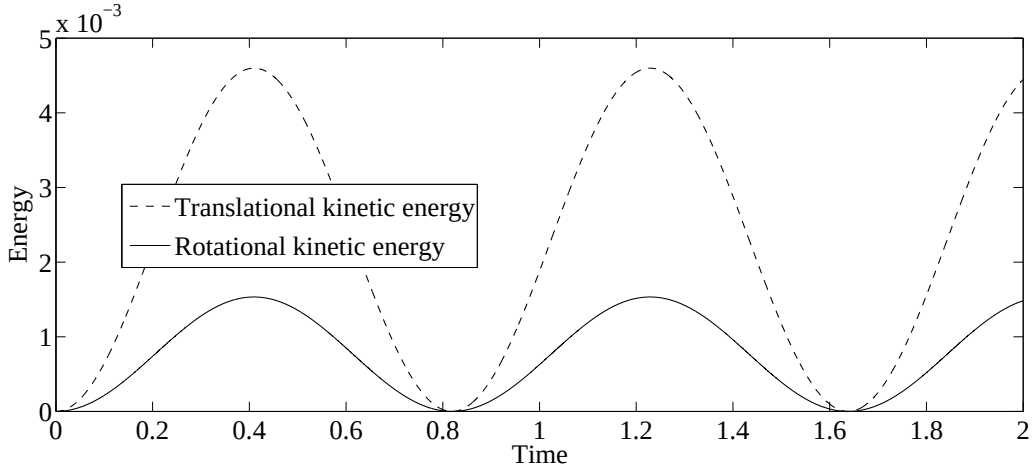

Figure 4.4: Translational and rotational kinetic energy over time

Chapter 5

Concluding Remarks and Future Work

A flexible fiber model, based on the concept of a chain of cylindrical segments, has been implemented in a general purpose CFD code. The model takes into account for the translational and rotational degrees of freedom of the segments, and ensures the fiber integrity. The model has been coupled with both imposed and simultaneously predicted 2D flow fields. The conclusions are that the fibers follow the flow and deform according to the flow gradients, and that the connectivity forces ensure the fiber integrity. Due to the present simplifications in the fiber model no further conclusions can be drawn at this time. A generic test case that resembles physical pendulum validates the fiber model motion concept through the energy conservation and response time. The on-going work is to couple the currently implemented fiber model with 3D flow fields. The next step is adding bending and twisting degrees of freedom as well as taking into account the interaction forces to make the fiber model more complete.

Bibliography

[1] R. F. Ross and D. J. Klingenberg. Dynamic simulation of flexible fibers composed of linked rigid bodies. *Journal of Chemical Physics*, 106:2949, 1997.

[2] Russel F. R. Klingenberg D.J. Skjetne, P. Dynamic simulation of flexible fibers composed of linked rigid bodies. *Journal of Chemical Physics*, 106:2949, 1997.

[3] T. Matsuoka and S. Yamamoto. Dynamic simulation of fiber suspensions in shear flow. *J. Chem. Phys.*, 102:2254, 1995.

[4] O. L. Forgacs and S. G. Mason. Particle motions in sheared suspensions: Ix.spin and deformation of threadlike particles. *Journal of Colloid Science*, 14:457–472, 1959.

[5] O. L. Forgacs and S. G. Mason. Particle motions in sheared suspensions: X.orbits of flexible threadlike particles. *Journal of Colloid Science*, 14:473–491, 1959.

[6] C.T Crowe, M. Sommerfeld, and Y. Tsuji. *Multiphase Flows With Droplets and Particles*. CRC,New York, 1998.

[7] Lindstrom S. B. and T. Uesaka. Simulation of the motion of flexible fibers in viscous fluid flow. *Physics of Fluids*, 19:113307, 2007.

[8] C. F. Schmid, L. H. Switzer, and Klingenberg D. J. Simulation of fiber flocculations:effects of fiber properties and interfiber friction. *J. Rheol.*, 44:781, 2000.

[9] S. Kim and Karilla S. J. *Microhydrodynamics: Principles and Selected Applications*. Butterworth-Heinemann, Stoneham, 1991.

[10] R. G. Cox. The motion og long slender bodies in a viscous fluid. part2. shear flow. *J. Fluid Mech.*, 45:625, 1971.

[11] D. J. Tritton. *Physical fluid dynamics*. Clarendon, Oxford, 2nd edition, 1988.

[12] P. Smith and R.C. Smith. *Mechanics*. John Wiley and Sons, 2nd edition, 1993.

Appendices

Appendix A

Tensor Calculus

The purpose of this appendix is to give an overview of the main vector and tensor operations, which are used in the fiber model equation derivation.

A.1 Vector and Tensor Notation

As it is well known in vector and tensor algebra a vector is represented by an ordered set of components, which represent its projections on the coordinate axes

$$\boldsymbol{a} = [a_1, a_2, a_3] \tag{A.1}$$

Another way of representing a vector is by the sum of the magnitudes of its projections on the three mutually perpendicular axes, i.e.

$$\boldsymbol{a} = a_1\boldsymbol{\delta}_1 + a_2\boldsymbol{\delta}_2 + a_3\boldsymbol{\delta}_3 \equiv a_i\boldsymbol{\delta}_i \tag{A.2}$$

A second-order tensor is represented by an ordered array of nine components, i.e.

$$\boldsymbol{T} = \begin{bmatrix} T_{11} & T_{12} & T_{13} \\ T_{21} & T_{22} & T_{23} \\ T_{31} & T_{32} & T_{33} \end{bmatrix} \tag{A.3}$$

One special second order tensor is the unit tensor or the identity tensor, i.e.

$$\boldsymbol{\delta} = \begin{bmatrix} 1 & 0 & 0 \\ 0 & 1 & 0 \\ 0 & 0 & 1 \end{bmatrix} \tag{A.4}$$

Its components can be defined using the Kronecker delta symbol as

$$\delta_{ij} = \begin{cases} 1, & if\ i = j \\ 0, & if\ i \neq j \end{cases} \tag{A.5}$$

A third-order tensor has 27 components and can be represented in index notation as P_{ijk}. The third order permutation tensor, or Levi-Civita tensor ϵ_{ijk} is defined by

$$\epsilon_{ijk} = \begin{cases} +1 & if\ \ (i,j,k) = (1,2,3),(3,1,2),\ \ or(2,3,1), \\ -1 & if\ \ (i,j,k) = (1,3,2),(3,2,1),\ \ or(2,1,3), \\ 0 & if\ \ i = j,\ \ or\ \ j = k,\ \ or\ \ k = i \end{cases} \tag{A.6}$$

A.2 Vector and Tensor Operations

The dot product of two vectors results in a scalar

$$\boldsymbol{a} \cdot \boldsymbol{b} = a_1 b_1 + a_2 b_2 + a_3 b_3 \equiv a_i b_i \tag{A.7}$$

The outer product of two vectors results in a tensor as

$$\boldsymbol{ab} = \begin{bmatrix} a_1 b_1 & a_1 b_2 & a_1 b_3 \\ a_2 b_1 & a_2 b_2 & a_2 b_3 \\ a_3 b_1 & a_3 b_2 & a_3 b_3 \end{bmatrix} = a_i b_j \tag{A.8}$$

The dot product of a tensor with a vector is given by

$$\boldsymbol{T} \cdot \boldsymbol{a} = \begin{pmatrix} T_{11} a_1 + T_{12} a_2 + T_{13} a_3 \\ T_{21} a_1 + T_{22} a_2 + T_{23} a_3 \\ T_{31} a_1 + T_{32} a_2 + T_{33} a_3 \end{pmatrix} = T_{ij} a_j \tag{A.9}$$

The dot product of a vector with a tensor is given by

$$\boldsymbol{a} \cdot \boldsymbol{T} = \begin{pmatrix} a_1 T_{11} + a_2 T_{21} + a_3 T_{31} \\ a_1 T_{12} + a_2 T_{22} + a_3 T_{32} \\ a_1 T_{13} + a_2 T_{23} + a_3 T_{33} \end{pmatrix} = a_j T_{ji} \tag{A.10}$$

In general $\boldsymbol{a} \cdot \boldsymbol{T} \neq \boldsymbol{T} \cdot \boldsymbol{a}$. If T is a symmetric tensor, $\boldsymbol{a} \cdot \boldsymbol{T} = \boldsymbol{T} \cdot \boldsymbol{a}$.
The dot product of two tensors $\boldsymbol{T}$ and $\boldsymbol{S}$ produces a tensor $\boldsymbol{P} = \boldsymbol{T} \cdot \boldsymbol{S}$, whose components are

$$P_{ij} = T_{ik} S_{kj} \tag{A.11}$$

The dot product of two tensors $\boldsymbol{T}$ and $\boldsymbol{S}$ produces a tensor $\boldsymbol{P} = \boldsymbol{T} \cdot \boldsymbol{S}$, whose components are given by

$$P_{ij} = T_{ik} S_{kj} \tag{A.12}$$

The double inner product of two second-order tensors $\boldsymbol{T}$ and $\boldsymbol{S}$ produces a scalar $s = \boldsymbol{T} : \boldsymbol{S}$, which is given as a sum of the nine products of the tensor components

$$\begin{aligned} s = T_{ij} S_{ij} = T_{11} S_{11} + T_{12} S_{12} + T_{13} S_{13} \\ + T_{21} S_{21} + T_{22} S_{22} + T_{23} S_{23} \\ + T_{31} S_{31} + T_{32} S_{32} + T_{33} S_{33} \end{aligned} \tag{A.13}$$

Another operation to be defined is the cross product. It is exclusive to vectors only. For two vectors $\boldsymbol{a}$ and $\boldsymbol{b}$, the cross product gives a vector $\boldsymbol{c} = \boldsymbol{a} \times \boldsymbol{b}$, whose components are

$$\boldsymbol{c} = \epsilon_{ijk} a_j b_k = (a_2 b_3 - a_3 b_2, a_3 b_1 - a_1 b_3, a_1 b_2 - a_2 b_1) \tag{A.14}$$

where ϵ_{ijk} is Levi-Civita permutation tensor.

A.3 Differential Operators

In the Cartesian coordinate system, the nabla operator is defined as

$$\nabla \equiv \boldsymbol{\delta}_1 \frac{\partial}{\partial x_1} + \boldsymbol{\delta}_2 \frac{\partial}{\partial x_2} + \boldsymbol{\delta}_3 \frac{\partial}{\partial x_3} \equiv \boldsymbol{\delta}_k \frac{\partial}{\partial x_k} \tag{A.15}$$

It can operate on any tensor field to produce a tensor field that is one order higher. The gradient of a vector field $\boldsymbol{a}$ is a second order tensor field, i.e.

$$\nabla \boldsymbol{a} = \boldsymbol{\delta}_1 \frac{\partial \boldsymbol{a}}{\partial x_1} + \boldsymbol{\delta}_2 \frac{\partial \boldsymbol{a}}{\partial x_2} + \boldsymbol{\delta}_3 \frac{\partial \boldsymbol{a}}{\partial x_3} \equiv \boldsymbol{\delta}_k \frac{\partial \boldsymbol{a}}{\partial x_k} \tag{A.16}$$

The divergence of a vector field $\boldsymbol{a}$, is a scalar field

$$\nabla \cdot \boldsymbol{a} = \frac{\partial a_1}{\partial x_1} + \frac{\partial a_2}{\partial x_2} + \frac{\partial a_3}{\partial x_3} \equiv \frac{\partial a_k}{\partial x_k} \tag{A.17}$$

The curl of a vector field $\boldsymbol{a}$ is a vector field defined as

$$\nabla \times \boldsymbol{a} = \epsilon_{ijk} \partial_j a_k = \left(\frac{\partial a_3}{\partial x_2} - \frac{\partial a_2}{\partial x_3}, \frac{\partial a_1}{\partial x_3} - \frac{\partial a_3}{\partial x_1}, \frac{\partial a_2}{\partial x_1} - \frac{\partial a_1}{\partial x_2} \right) \tag{A.18}$$

where ϵ_{ijk} is Levi-Civita permutation tensor.

Appendix B

Inertia of a Rotating Cylinder

In this appendix the inertia of a rotating cylinder is discussed. Firstly, the concept of the inertia tensor will be introduced, starting from an expression for the angular momentum of a 3D rigid body. Then, the derivation of the inertia tensor for a cylinder is presented.

B.1 Tensor of Inertia

The expression for the angular momentum of a system of particles about their center of mass is given by [12]

$$\boldsymbol{L} = \sum_{k=1}^{N} (\boldsymbol{r}_i \times m_i(\boldsymbol{\omega} \times \boldsymbol{r}_i)) \tag{B.1}$$

The integral stands for a summation in the case of a continuum distribution of mass and Eq.B.1 can be written as

$$\boldsymbol{L} = \int_m \boldsymbol{r} \times (\boldsymbol{\omega} \times \boldsymbol{r}) dm = \int_m [(\boldsymbol{r} \cdot \boldsymbol{r})\, \boldsymbol{\omega} - (\boldsymbol{r} \cdot \boldsymbol{\omega})\, \boldsymbol{r}] dm \tag{B.2}$$

where, $\boldsymbol{r}$ and $\boldsymbol{\omega}$ are the position vector and the angular velocity vector relative to the center of mass, respectively. In Cartesian coordinates, $\boldsymbol{r} = x\boldsymbol{i} + y\boldsymbol{j} + z\boldsymbol{k}$ and $\boldsymbol{\omega} = \omega_x\boldsymbol{i} + \omega_y\boldsymbol{j} + \omega_z\boldsymbol{k}$, and the expression above

yields

$$\begin{aligned}\boldsymbol{L} &= \left(\omega_x \int_m \left(x^2+y^2+z^2\right) - \int_m \left(\omega_{\mathrm{x}} x + \omega_{\mathrm{y}} y + \omega_{\mathrm{z}} z\right) x dm\right) \boldsymbol{i} \\ &+ \left(\omega_y \int_m \left(x^2+y^2+z^2\right) - \int_m \left(\omega_{\mathrm{x}} x + \omega_{\mathrm{y}} y + \omega_{\mathrm{z}} z\right) y dm\right) \boldsymbol{j} \\ &+ \left(\omega_z \int_m \left(x^2+y^2+z^2\right) - \int_m \left(\omega_{\mathrm{x}} x + \omega_{\mathrm{y}} y + \omega_{\mathrm{z}} z\right) z dm\right) \boldsymbol{k} \\ &= \left(I_{xx}\omega_x + I_{xy}\omega_y + I_{xz}\omega_z\right) \boldsymbol{i} \\ &+ \left(I_{yx}\omega_x + I_{yy}\omega_y + I_{yz}\omega_z\right) \boldsymbol{j} \\ &+ \left(I_{zx}\omega_x + I_{zy}\omega_y + I_{zz}\omega_z\right) \boldsymbol{k}\end{aligned} \tag{B.3}$$

The quantities I_{xx}, I_{yy}, and I_{zz} are called moments of inertia with respect to the x, y and z axis, respectively, and are given by

$$I_{xx} = \int_m \left(y^2+z^2\right) dm, \qquad I_{yy} = \int_m \left(x^2+z^2\right) dm, \qquad I_{zz} = \int_m \left(x^2+y^2\right) dm$$

The terms $I_{xy}, I_{xz}, I_{yx}, I_{yz}, I_{zx}$ and I_{zy} are called products of inertia and are given by

$$I_{xy} = I_{yx} = \int_m (xy) dm, \qquad I_{xz} = I_{zx} = \int_m xz dm, \qquad I_{yz} = I_{zy} = \int_m yz dm$$

The quantity reflecting the rotational inertia $\boldsymbol{I}$ is a second order tensor. In the notation of linear algebra Eq.B.3 reads

$$\begin{pmatrix} L_x \\ L_y \\ L_z \end{pmatrix} = \begin{pmatrix} I_{xx} & I_{xy} & I_{xz} \\ I_{yx} & I_{yy} & I_{yz} \\ I_{zx} & I_{zy} & I_{zz} \end{pmatrix} \begin{pmatrix} \omega_x \\ \omega_y \\ \omega_z \end{pmatrix} \tag{B.4}$$

The components of the inertia tensor $\boldsymbol{I}$ have a physical meaning. For example, spinning the object around the y axis, the x component of angular momentum is $L_x = I_{xy}\omega_y$. If the angular velocity has all three components, the x component of $\boldsymbol{L}$ will equal $L_x = I_{xx}\omega_x + I_{xy}\omega_y + I_{xz}\omega_z$.

B.2 Inertia of a Rotating Cylinder

A cylinder of constant radius R, length l and density ρ is here considered. The origin of the coordinate system is choosen at the center of mass of the cylinder and the z axis of the coordinate system is parallel

to the axis of the cylinder. The components of the inertia tensor can be computed using polar coordinate system $\overrightarrow{r} = (r\cos\theta, r\sin\theta, z)$ in the xy plane. The I_{xx} component of the inertia tensor is given by

$$\begin{aligned} I_{xx} &= \rho \int_{-l/2}^{l/2} dz \int_0^{2\pi} d\theta \int_0^R r(r^2\sin^2\theta + z^2)dr \\ &= \rho \left[\int_{-l/2}^{l/2} z^2 dz \int_0^{2\pi} d\theta \int_0^R r dr + \int_{-l/2}^{l/2} dz \int_0^{2\pi} \sin^2\theta d\theta \int_0^R r^3 dr \right] \end{aligned} \tag{B.5}$$

The density is $\rho = m/\pi l R^2$, thus

$$I_{xx} = \frac{1}{12}ml^2 + \frac{1}{4}mR^2 \tag{B.6}$$

The two other moments of inertia are

$$\begin{aligned} I_{yy} &= \frac{m}{\pi R^2 l} \int_{-l/2}^{l/2} dz \int_0^{2\pi} d\theta \int_0^R r(r^2\cos^2\theta + z^2)dr \\ &= \frac{1}{12}ml^2 + \frac{1}{4}mR^2 = I_{xx} \end{aligned} \tag{B.7}$$

and

$$\begin{aligned} I_{zz} &= \frac{m}{\pi R^2 l} \int_{-l/2}^{l/2} dz \int_0^{2\pi} d\theta \int_0^R r(r^2\cos^2\theta + r^2\sin^2\theta)dr \\ &= \int_{-l/2}^{l/2} dz \int_0^{2\pi} d\theta \int_0^R r^3 dr = \frac{1}{2}mR^2 \end{aligned} \tag{B.8}$$

The calculation of the products of inertia is analogous.

$$I_{xy} = I_{yx} = -\frac{m}{\pi R^2 l} \int_{-l/2}^{l/2} dz \int_0^{2\pi} d\theta \int_0^R r^3 \sin\theta\cos\theta dr = 0 \tag{B.9}$$

because $\int_0^{2\pi} \cos\theta\sin\theta d\theta = 0$. Similarly

$$I_{xz} = I_{zx} = -\frac{m}{\pi R^2 l} \int_{-l/2}^{l/2} dz \int_0^{2\pi} d\theta \int_0^R zr^2\cos\theta dr = 0 \tag{B.10}$$

and

$$I_{yz} = I_{zy} = -\frac{m}{\pi R^2 l} \int_{-l/2}^{l/2} dz \int_0^{2\pi} d\theta \int_0^R zR^2\sin\theta dr = 0 \tag{B.11}$$

because $\int_0^{2\pi} \cos\theta d\theta = 0$ and $\int_0^{2\pi} \sin\theta d\theta = 0$. The inertia tensor for a cylinder, rotating around its center of mass can thus be written as [7]

$$\boldsymbol{I} = \frac{1}{12} m \left(l^2 + 3R^2\right) \left[\, \boldsymbol{\delta} - \hat{\boldsymbol{z}}\hat{\boldsymbol{z}}\right] + \frac{1}{2} m R^2 \hat{\boldsymbol{z}}\hat{\boldsymbol{z}} \tag{B.12}$$

The time derivative of the tensor of inertia is

$$\begin{aligned} &\frac{\partial}{\partial t} \left\{ \frac{1}{12} m \left(l^2 + 3R^2\right) \left[\, \boldsymbol{\delta} - \hat{\boldsymbol{z}}\hat{\boldsymbol{z}}\right] + \frac{1}{2} m R^2 \hat{\boldsymbol{z}}\hat{\boldsymbol{z}} \right\} \\ &= \frac{1}{12} m \left(3R^2 - l^2\right) \frac{\partial}{\partial t} \left(\hat{\boldsymbol{z}}\hat{\boldsymbol{z}}\right) \end{aligned} \tag{B.13}$$

A straight-forward differentiation gives the components of $\dot{\boldsymbol{I}}$ as

$$\begin{aligned} \dot{I}_{ij} =& \frac{1}{12} m \left(3R^2 - l^2\right) \frac{\partial}{\partial t} \left(z_i z_j\right) \\ &= \frac{1}{12} m \left(3R^2 - l^2\right) \left(\dot{z}_i z_j + z_i \dot{z}_j\right) \\ &= \frac{1}{12} m \left(3R^2 - l^2\right) \left[\left(\boldsymbol{\omega} \times \hat{\boldsymbol{z}}\right)_i z_j + z_i \left(\boldsymbol{\omega} \times \hat{\boldsymbol{z}}\right)_j\right] \\ &= \frac{1}{12} m \left(l^2 - 3R^2\right) \left[\left(\hat{\boldsymbol{z}} \times \boldsymbol{\omega}\right)_i z_j + z_i \left(\hat{\boldsymbol{z}} \times \boldsymbol{\omega}\right)_j\right] \end{aligned} \tag{B.14}$$

Finally, the time derivative of the tensor of inertia $\dot{\boldsymbol{I}}$ is given by

$$\dot{\boldsymbol{I}} = \frac{1}{12} m \left(l^2 - 3R^2\right) \left\{ \left[\left(\hat{\boldsymbol{z}} \times \boldsymbol{\omega}\right) \hat{\boldsymbol{z}}\right] + \left[\left(\hat{\boldsymbol{z}} \times \boldsymbol{\omega}\right) \hat{\boldsymbol{z}}\right]^{\mathrm{T}} \right\} \tag{B.15}$$

Appendix C

Numerics

This appendix discusses different numerical issues related to the implementation of the fiber model. A short overview of dimensional analysis and scaling is first given. Ill-conditioned linear systems are then discussed, followed by Tikhonov regularization as one possible method to solve such systems.

C.1 Dimensional Analysis and Scaling

A mathematical model describes the behavior of a real physical system in terms of mathematical equations. These equations represent the relation between the relevant properties of the system under consideration. The models include variables and parameters. If the variables or parameters in a model correspond to physical properties, they have physical dimensions. The fundamental dimensions, introduced by Maxwell include mass, length and time. The dimensions of any physical quantity can be expressed in terms of the fundamental dimensions. In other cases the dimensionality of a quantity is deduced from the rule that all terms in a particular equation must have the same dimension. This rule is a consequence of the condition that the form of any equation in a mathematical model may not depend on the units used. For example, the dimension of force directly follows from Newton's second law, which states that, for a single mass, the mass times the accelaration equals the total force exerted on the mass. This means that the dimension of a force F, denoted as $[F]$ equals the dimension $[ma]$ of the product of mass m and acceleration a. For any dimensionless quantity, q, $[q] = 1$. The fact that the variables and parameters have physical dimensions can be very useful. The techniques of dimensional analysis and scaling are powerful tools to analyze the models. The basic idea is to apply a transformation to the variables and parameters, that will

result in simplified equations. Nondimensionalizing a mathematical model is a constructive way to formulate the model in terms of dimensionless quantities only. The basic idea is to apply a transformation to the variables and parameters, that will result in simplified equations. Reduction of parameters has also the purpose of scaling. These techniques can also provide the information on which combination of parameters the system depends. The total number of variables and/or parameters is minimal. However, dimensional analysis is more general than scaling since it is based on the transformation of both variables and parameters, whereas in scaling only the variables are transformed. Another difference is that dimensional analysis starts basically from the dimensions involved in the system and may predict some of its features without knowing the model equations, while the scaling starts from the governing equations.

C.2 Ill-Conditioned Linear System

An $n \times n$ linear system $\boldsymbol{A} \cdot \boldsymbol{x} = \boldsymbol{b}$ is considered. The solution vector $\boldsymbol{x}$ of this system is guaranteed to exist and to be unique if the coefficient array $\boldsymbol{A}$ is invertible. The solution vector $\boldsymbol{x}$ can be formulated in terms of the inverse of the coefficient array $\boldsymbol{A}$ and the right-hand-side vector $\boldsymbol{b}$ as $\boldsymbol{x} = \boldsymbol{A}^{-1}\boldsymbol{b}$. This relationship provides a concise mathematical representation of the solution, but it is seldom used in practice since the array inversion is computationally expensive. An alternative way to describe the existence of a solution is to say that the system $\boldsymbol{A} \cdot \boldsymbol{x} = \boldsymbol{b}$ is solvable if and only if the vector $\boldsymbol{b}$ may be expressed as a linear combination of the columns of $\boldsymbol{A}$. The invertability of the coefficient array $\boldsymbol{A}$ may ensure that a solution exists, but it does not help in determining the solution. Some systems can be solved accurately using numerical methods while others can not. In order to better understand the accuracy of a numerical solution, the condition of the system can be classified. Conditioning is a property of a matrix $\boldsymbol{A}$ that determines whether it can be expected that any numerical algorithm can provide numerical solution to a linear system involving $\boldsymbol{A}$. Any linear system represented on a computer has a certain error, since a fixed precision is used. This means that a linear system $\boldsymbol{A} \cdot \boldsymbol{x} = \boldsymbol{b}$ becomes a slightly pertubed system $\hat{\boldsymbol{A}} \cdot \hat{\boldsymbol{x}} = \hat{\boldsymbol{b}}$, when represented on a computer. When the solution is highly sensitive to the values of the coefficients matrix $\boldsymbol{A}$ or the right-hand-side vector $\boldsymbol{b}$, meaning that small perturbations in $\boldsymbol{b}$ can produce large changes in $\boldsymbol{x}$, the equations are called ill-conditioned. In order to investigate how a small change in $\boldsymbol{b}$ changes the solution vector $\boldsymbol{x}$, let $\boldsymbol{x} + \Delta\boldsymbol{x}$ denote the solution when $\boldsymbol{b}$ changes from $\boldsymbol{b}$ to $\boldsymbol{b} + \Delta\boldsymbol{b}$.

It can be written as

$$\boldsymbol{A}(\boldsymbol{x}+\Delta\boldsymbol{x}) = \boldsymbol{b}+\Delta\boldsymbol{b} \Rightarrow \boldsymbol{A}\Delta\boldsymbol{x} = \Delta\boldsymbol{b} \Rightarrow \Delta\boldsymbol{x} = \boldsymbol{A}^{-1}\Delta\boldsymbol{b}$$

By using the norm property $\|\boldsymbol{A}\cdot\boldsymbol{x}\| \leq \|\boldsymbol{A}\|\cdot\|\boldsymbol{x}\|$ it follows

$$\|\boldsymbol{A}^{-1}\Delta\boldsymbol{b}\| \leq \|\boldsymbol{A}^{-1}\|\cdot\|\Delta\boldsymbol{b}\| \Rightarrow \|\Delta x\| \leq \|\boldsymbol{A}^{-1}\|\cdot\|\Delta\boldsymbol{b}\| \tag{C.1}$$

Applying the same property to the original system gives

$$\|\boldsymbol{A}\cdot\boldsymbol{x}\| \leq \|\boldsymbol{A}\|\cdot\|\boldsymbol{x}\| \Rightarrow \|\boldsymbol{b}\| \leq \|\boldsymbol{A}\|\cdot\|\boldsymbol{x}\| \Leftrightarrow \|\boldsymbol{A}\|\cdot\|\boldsymbol{x}\| \geq \|\boldsymbol{b}\| \tag{C.2}$$

Dividing EqC.1 by Eq C.2 leads to

$$\begin{aligned}\frac{\|\Delta\boldsymbol{x}\|}{\|\boldsymbol{A}\|\cdot\|\boldsymbol{x}\|} \leq \frac{\|\boldsymbol{A}^{-1}\|\cdot\|\Delta\boldsymbol{b}\|}{\|\boldsymbol{b}\|} &\Rightarrow \frac{\Delta\boldsymbol{x}}{\boldsymbol{x}} \leq \|\boldsymbol{A}\|\|\boldsymbol{A}^{-1}\|\frac{\|\Delta\boldsymbol{b}\|}{\|\boldsymbol{b}\|} \\ &\Leftrightarrow \frac{\Delta\boldsymbol{x}}{\boldsymbol{x}} \leq K(\boldsymbol{A})\frac{\|\Delta\boldsymbol{b}\|}{\|\boldsymbol{b}\|}\end{aligned} \tag{C.3}$$

where $K(\boldsymbol{A})$ is called the condition number of the matrix $\boldsymbol{A}$ and is defined as $K(\boldsymbol{A}) = \|\boldsymbol{A}\|\|\boldsymbol{A}^{-1}\|$, where $\|\boldsymbol{A}\| = \max_{k=1}^{N}\{\sum_{j=1}^{N}|A_{kj}|\}$ and provided $\boldsymbol{A}$ is nonsingular. When the condition number $K(\boldsymbol{A})$ becomes large, the system is regarded as being ill-conditioned. Matrices with condition number 1 are said to be well-conditioned. However, there is no clear threshold how large $K(\boldsymbol{A})$ should be before a system is regarded as ill-conditioned. In order to assess the effects of ill-conditioning, a rule of thumb can be used. For a system with condition number $K(\boldsymbol{A})$, a loss of roughly $\log_{10}K(\boldsymbol{A})$ decimal places in the accuracy of the solution is expected.

C.3 Tikhonov Regularization

Tikhonov regularization is one of the common methods of regularization of ill-posed problems. The purpose of this regularization is to improve the conditioning of the problem and enable a numerical solution. An explicit solution $\hat{x}$ is given by

$$\hat{\boldsymbol{x}} = \left(\boldsymbol{A}^T\boldsymbol{A} + \boldsymbol{\Gamma}^T\boldsymbol{\Gamma}\right)^{-1}\boldsymbol{A}^T\boldsymbol{b} \tag{C.4}$$

In many cases, matrix $\boldsymbol{\Gamma}$ is choosen as the identity matrix in order to give preference to the solutions with the smaller norms.

Appendix D

Dimensionless Governing Equations

This Appendix presents complete derivation of a dimensionless set of governing equations for the fiber model described in Chapter 2.

D.0.1 Dimensionless Linear Momentum Equation

The discretized linear momentum equation reads

$$\frac{m}{\Delta t}(\dot{\boldsymbol{r}}_{i,n} - \dot{\boldsymbol{r}}_{i,n-1}) = (\boldsymbol{A}^{v}_{i,n-1} + \boldsymbol{A}^{I}_{i,n-1}) \cdot [\boldsymbol{v}(\boldsymbol{r}_{i,n-1}) - \dot{\boldsymbol{r}}_{i,n}] + \boldsymbol{X}_{i+1,n} - \boldsymbol{X}_{i,n} \tag{D.1}$$

All the forces are here scaled with the factor $3\pi\eta l r\dot{\gamma}$ [8], which has units of force $[kgm/s^2] \equiv [N]$, where $\dot{\gamma}$ is a scalar related to the rate of deformation tensor by $\dot{\gamma} = \sqrt{1/2(\boldsymbol{\gamma} : \boldsymbol{\gamma})}$ and $:$ is the double inner product operator described in Appendix A. The time is scaled with the inverse of the shear rate $1/\dot{\gamma}$ $[s]$, the velocities are scaled with $r\dot{\gamma}$ $[m/s]$ and the hydrodynamic resistance tensors with $3\pi\eta l$ $[kg/s]$. The scale factor for the mass is $3\pi\eta l/\dot{\gamma}$ $[kg]$. Applying the scaling to Eq.D.1 yields

$$\begin{aligned}\frac{m}{\frac{3\pi\eta l}{\dot{\gamma}}} \frac{1}{\frac{\Delta t}{1/\dot{\gamma}}} \frac{(\dot{\boldsymbol{r}}_{i,n} - \dot{\boldsymbol{r}}_{i,n-1})}{r\dot{\gamma}} &= \frac{(\boldsymbol{A}^{v}_{i,n-1} + \boldsymbol{A}^{I}_{i,n-1})}{3\pi\eta l} \cdot \frac{[\boldsymbol{v}(\boldsymbol{r}_{i,n-1}) - \dot{\boldsymbol{r}}_{i,n}]}{r\dot{\gamma}} \\ &+ \frac{(\mathbf{X}_{i+1,n} - \mathbf{X}_{i,n})}{3\pi\eta l r\dot{\gamma}}\end{aligned} \tag{D.2}$$

The corresponding dimensionless variables are given as

$$\begin{aligned}
&\boldsymbol{X}^*_{i,n} = \frac{\boldsymbol{X}_{i,n}}{3\pi\eta l r\dot{\gamma}} \\
&m^* = \frac{m}{\frac{3\pi\eta l}{\dot{\gamma}}} \;\; ; \;\; \Delta t^* = \frac{\Delta t}{\frac{1}{\dot{\gamma}}} \\
&\boldsymbol{v}^*\left(\boldsymbol{r}^*_{i,n-1}\right) = \frac{\boldsymbol{v}\left(\boldsymbol{r}_{i,n-1}\right)}{r\dot{\gamma}} \;\; ; \;\; \dot{\boldsymbol{r}}^*_{i,n-1} = \frac{\dot{\boldsymbol{r}}_{i,n-1}}{r\dot{\gamma}} \;\; ; \;\; \dot{\boldsymbol{r}}^*_{i,n} = \frac{\dot{\boldsymbol{r}}_{i,n}}{r\dot{\gamma}} \\
&\boldsymbol{A}^{v*}_{i,n-1} = \frac{\boldsymbol{A}^{v}_{i,n-1}}{3\pi\eta l} = [Y^A\boldsymbol{\delta} + (X^A - Y^A)\hat{\boldsymbol{z}}_{i,n-1}\hat{\boldsymbol{z}}_{i,n-1}] \\
&\boldsymbol{A}^{I*}_{i,n-1} = \frac{\boldsymbol{A}^{I}_{i,n-1}}{3\pi\eta l} = \frac{\frac{1}{2}C^I_D\rho d v^*_{\perp,i}}{3\pi\eta}[\boldsymbol{\delta} - \hat{\boldsymbol{z}}_{i,n-1}\hat{\boldsymbol{z}}_{i,n-1}]
\end{aligned}$$

After replacing the dimensionless variables, the dimensionless discretized linear momentum equation reads

$$\frac{m^*}{\Delta t^*}(\dot{\boldsymbol{r}}^*_{i,n} - \dot{\boldsymbol{r}}^*_{i,n-1}) = (\boldsymbol{A}^{v*}_{i,n-1} + \boldsymbol{A}^{I*}_{i,n-1})\cdot[\boldsymbol{v}^*(\boldsymbol{r}^*_{i,n-1}) - \dot{\boldsymbol{r}}^*_{i,n}] + \boldsymbol{X}^*_{i+1,n} - \boldsymbol{X}^*_{i,n} \quad \text{(D.3)}$$

The dimensionless translational velocity for segment i is then given by

$$\begin{aligned}
\dot{\boldsymbol{r}}^*_{i,n} =& (\frac{m^*}{\Delta t^*}\boldsymbol{\delta} + \boldsymbol{A}^{v*}_{i,n-1} + \boldsymbol{A}^{I*}_{i,n-1})^{-1} \cdot \big(\frac{m^*}{\Delta t^*}\dot{\boldsymbol{r}}^*_{i,n-1} + (\boldsymbol{A}^{v*}_{i,n-1} + \boldsymbol{A}^{I*}_{i,n-1})\cdot \\
& \boldsymbol{v}^*(\boldsymbol{r}^*_{i,n-1}) + \boldsymbol{X}^*_{i+1,n} - \boldsymbol{X}^*_{i,n}\big)
\end{aligned} \quad \text{(D.4)}$$

D.0.2 Dimensionless Angular Momentum Equation

The discretized angular momentum equation for fiber segment i is given by

$$\begin{aligned}
&\dot{\boldsymbol{I}}_{i,n-1}\cdot\boldsymbol{\omega}_{i,n} + \frac{1}{\Delta t}\dot{\boldsymbol{I}}_{i,n-1}\cdot(\boldsymbol{\omega}_{i,n} - \boldsymbol{\omega}_{i,n-1}) = \left(\boldsymbol{C}^v_{i,n-1} + \boldsymbol{C}^I_{i,n-1}\right)\cdot \\
&[\boldsymbol{\Omega}\left(\boldsymbol{r}_{i,n-1}\right) - \boldsymbol{\omega}_{i,n}] + \left(\boldsymbol{H}^v_{i,n-1} + \boldsymbol{H}^I_{i,n-1}\right) : \dot{\boldsymbol{\gamma}}\left(\boldsymbol{r}_{i,n-1}\right) \\
&+ \frac{l_i}{2}\hat{\boldsymbol{z}}_{i,n-1}\times\boldsymbol{X}_{i+1,n} + \left(\frac{-l_i}{2}\hat{\boldsymbol{z}}_{i,n-1}\right)\times(-\boldsymbol{X}_{i,n})
\end{aligned} \quad \text{(D.5)}$$

All the torques are scaled by the factor $\pi\eta l^3\dot{\gamma}$ [8] that has units of torque $[kgm^2/s^2] = [Nm]$, yielding

$$\begin{aligned}
&\frac{\dot{\boldsymbol{I}}_{i,n-1}}{\pi\eta l^3}\cdot\frac{\boldsymbol{\omega}_{i,n}}{\dot{\gamma}}+\frac{1}{\frac{\Delta t}{1/\dot{\gamma}}}\frac{\boldsymbol{I}_{i,n-1}}{\frac{\pi\eta l^3}{\dot{\gamma}}}\cdot\frac{(\boldsymbol{\omega}_{i,n}-\boldsymbol{\omega}_{i,n-1})}{\dot{\gamma}}=\frac{\left(\boldsymbol{C}^{\upsilon}_{i,n-1}+\boldsymbol{C}^{I}_{i,n-1}\right)}{\pi\eta l^3}\cdot\\
&\frac{[\boldsymbol{\Omega}\left(\boldsymbol{r}_{i,n-1}\right)-\boldsymbol{\omega}_{i,n}]}{\dot{\gamma}}+\frac{\left(\boldsymbol{H}^{\upsilon}_{i,n-1}+\boldsymbol{H}^{I}_{i,n-1}\right)}{\pi\eta l^3}:\frac{\dot{\boldsymbol{\gamma}}\left(\boldsymbol{r}_{i,n-1}\right)}{\dot{\gamma}}\\
&+\frac{\frac{l}{2}\hat{\boldsymbol{z}}_{i,n-1}\times\left(\boldsymbol{X}_{i+1,n}+\boldsymbol{X}_{i,n}\right)}{\pi\eta l^3\dot{\gamma}}
\end{aligned}\tag{D.6}$$

In analogy with the linear momentum equation the corresponding dimensionless variables are given by

$$\begin{aligned}
&\boldsymbol{\omega}^*_{i,n}=\frac{\boldsymbol{\omega}_{i,n}}{\dot{\gamma}}\ ;\ \boldsymbol{\omega}^*_{i,n-1}=\frac{\boldsymbol{\omega}_{i,n-1}}{\dot{\gamma}}\ ;\ \boldsymbol{I}^*_{i,n-1}=\frac{\boldsymbol{I}_{i,n-1}}{\pi\eta l^3/\dot{\gamma}}\ ;\ \dot{\boldsymbol{I}}^*_{i,n-1}=\frac{\dot{\boldsymbol{I}}_{i,n-1}}{\pi\eta l^3}\\
&\boldsymbol{C}^{\upsilon *}_{i,n-1}=\frac{\boldsymbol{C}^{\upsilon}_{i,n-1}}{\pi\eta l^3}=[Y^A\boldsymbol{\delta}+(X^A-Y^A)\hat{\boldsymbol{z}}_{i,n-1}\hat{\boldsymbol{z}}_{i,n-1}]\\
&\boldsymbol{C}^{I*}_{i,n-1}=\frac{\boldsymbol{C}^{I}_{i,n-1}}{\pi\eta l^3}=\frac{\frac{1}{24}C^I_D\rho d v^*_{\perp,i}}{\pi\eta\dot{\gamma}}[\boldsymbol{\delta}-\hat{\boldsymbol{z}}_{i,n-1}\hat{\boldsymbol{z}}_{i,n-1}]\\
&\boldsymbol{H}^{\upsilon *}_{i,n-1}=\frac{\boldsymbol{H}^{\upsilon}_{i,n-1}}{\pi\eta l^3}=-Y^H\left(\boldsymbol{\epsilon}\cdot\hat{\boldsymbol{z}}_{i,n-1}\right)\hat{\boldsymbol{z}}_{i,n-1}\\
&\boldsymbol{H}^{I*}_{i,n-1}=\frac{\boldsymbol{H}^{I}_{i,n-1}}{\pi\eta l^3}=-\frac{\frac{1}{24}C^I_D\rho d v^*_{\perp,i}}{\pi\eta\dot{\gamma}}[\left(\boldsymbol{\epsilon}\cdot\hat{\boldsymbol{z}}_{i,n-1}\right)\hat{\boldsymbol{z}}_{i,n-1}]\\
&\dot{\boldsymbol{\gamma}}^*\left(\boldsymbol{r}^*_{i,n-1}\right)=\frac{\dot{\boldsymbol{\gamma}}\left(\boldsymbol{r}_{i,n-1}\right)}{\dot{\gamma}}
\end{aligned}$$

The discretized dimensionless angular momentum equation for a fiber segment i can then be rewritten as

$$\begin{aligned}
&\left(\dot{\boldsymbol{I}}^*_{i,n-1}+\frac{1}{\Delta t^*}\boldsymbol{I}^*_{i,n-1}+\boldsymbol{C}^{\upsilon *}_{i,n-1}+\boldsymbol{C}^{I*}_{i,n-1}\right)\cdot\boldsymbol{\omega}^*_{i,n}=\frac{1}{\Delta t^*}\boldsymbol{I}^*_{i,n-1}\cdot\boldsymbol{\omega}^*_{i,n-1}\\
&+\left(\boldsymbol{C}^{\upsilon *}_{i,n-1}+\boldsymbol{C}^{I*}_{i,n-1}\right)\cdot\boldsymbol{\Omega}^*\left(\boldsymbol{r}^*_{i,n-1}\right)+\left(\boldsymbol{H}^{\upsilon *}_{i,n-1}+\boldsymbol{H}^{I*}_{i,n-1}\right):\dot{\boldsymbol{\gamma}}^*\left(\boldsymbol{r}^*_{i,n-1}\right)\\
&+\frac{3}{4r_p}\hat{\boldsymbol{z}}_{i,n-1}\times\left(\boldsymbol{X}^*_{i+1,n}+\boldsymbol{X}^*_{i,n}\right)
\end{aligned}\tag{D.7}$$

where $r_p = l/d$ is a segment aspect ratio. The dimensionless angular velocity for segment i reads

$$\boldsymbol{\omega}^*_{i,n} = \left(\dot{\boldsymbol{I}}^*_{i,n-1} + \frac{1}{\Delta t^*}\boldsymbol{I}^*_{i,n-1} + \boldsymbol{C}^{\upsilon *}_{i,n-1} + \boldsymbol{C}^{I*}_{i,n-1}\right)^{-1} \cdot \\ \left(\frac{1}{\Delta t^*}\boldsymbol{I}^*_{i,n-1}\cdot\boldsymbol{\omega}^*_{i,n-1} + \left(\boldsymbol{C}^{\upsilon *}_{i,n-1} + \boldsymbol{C}^{I*}_{i,n-1}\right)\cdot\boldsymbol{\Omega}^*\left(\boldsymbol{r}^*_{i,n-1}\right)\right. \\ \left. + \left(\boldsymbol{H}^{\upsilon *}_{i,n-1} + \boldsymbol{H}^{I*}_{i,n-1}\right) : \dot{\boldsymbol{\gamma}}^*\left(\boldsymbol{r}^*_{i,n-1}\right) + \frac{3}{4r_p}\boldsymbol{C}^{*}_{\boldsymbol{z}\,i,n-1}\cdot\left(\boldsymbol{X}^*_{i+1,n} + \boldsymbol{X}^*_{i,n}\right)\right) \quad \text{(D.8)}$$

where $\boldsymbol{C}^{*}_{\boldsymbol{z}\,i,n-1}$ is a second order tensor, which is a function of tensor $\left(\dot{\boldsymbol{I}}^*_{i,n-1} + \frac{1}{\Delta t^*}\boldsymbol{I}^*_{i,n-1} + \boldsymbol{C}^{\upsilon *}_{i,n-1} + \boldsymbol{C}^{I*}_{i,n-1}\right)^{-1}$ and the orientation vector $\hat{\boldsymbol{z}}_{i,n-1}$. Denoting $\boldsymbol{C}^{*}_{\boldsymbol{I}\,i,n-1} = \left(\dot{\boldsymbol{I}}^*_{i,n-1} + \frac{1}{\Delta t^*}\boldsymbol{I}^*_{i,n-1} + \boldsymbol{C}^{\upsilon *}_{i,n-1} + \boldsymbol{C}^{I*}_{i,n-1}\right)^{-1}$, the components of $\boldsymbol{C}^{*}_{\boldsymbol{z}\,i,n-1}$ are

$C^*_{z\,i,n-1,11} = C^*_{I\,i,n-1,22}\hat{z}^2_{i,n-1,3} - C^*_{I\,i,n-1,23}\hat{z}_{i,n-1,2}\hat{z}_{i,n-1,3} - C^*_{I\,i,n-1,32}\hat{z}_{i,n-1,3}\hat{z}_{i,n-1,2} + C^*_{I\,i,n-1,33}\hat{z}^2_{i,n-1,2}$

$C^*_{z\,i,n-1,12} = -C^*_{I\,i,n-1,21}\hat{z}^2_{i,n-1,3} + C^*_{I\,i,n-1,23}\hat{z}_{i,n-1,1}\hat{z}_{i,n-1,3} + C^*_{I\,i,n-1,31}\hat{z}_{i,n-1,2}\hat{z}_{i,n-1,3} - C^*_{I\,i,n-1,33}\hat{z}_{i,n-1,1}\hat{z}_{i,n-1,2}$

$C^*_{z\,i,n-1,13} = C^*_{I\,i,n-1,21}\hat{z}_{i,n-1,2}\hat{z}_{i,n-1,3} - C^*_{I\,i,n-1,22}\hat{z}_{i,n-1,1}\hat{z}_{i,n-1,3} - C^*_{I\,i,n-1,31}\hat{z}^2_{i,n-1,2} + C^*_{I\,i,n-1,32}\hat{z}_{i,n-1,1}\hat{z}_{i,n-1,2}$

$C^*_{z\,i,n-1,21} = C^*_{I\,i,n-1,32}\hat{z}_{i,n-1,3}\hat{z}_{i,n-1,1} - C^*_{I\,i,n-1,33}\hat{z}_{i,n-1,1}\hat{z}_{i,n-1,2} - C^*_{I\,i,n-1,12}\hat{z}^2_{i,n-1,3} + C^*_{I\,i,n-1,13}\hat{z}_{i,n-1,2}\hat{z}_{i,n-1,3}$

$C^*_{z\,i,n-1,22} = -C^*_{I\,i,n-1,31}\hat{z}_{i,n-1,1}\hat{z}_{i,n-1,3} + C^*_{I\,i,n-1,33}\hat{z}^2_{i,n-1,1} + C^*_{I\,i,n-1,1}\hat{z}^2_{i,n-1,3} - C^*_{I\,i,n-1,13}\hat{z}_{i,n-1,1}\hat{z}_{i,n-1,3}$

$C^*_{z\,i,n-1,23} = C^*_{I\,i,n-1,31}\hat{z}_{i,n-1,1}\hat{z}_{i,n-1,2} - C^*_{I\,i,n-1,32}\hat{z}^2_{i,n-1,1} - C^*_{I\,i,n-1,11}\hat{z}_{i,n-1,2}\hat{z}_{i,n-1,3} + C^*_{I\,i,n-1,12}\hat{z}_{i,n-1,1}\hat{z}_{i,n-1,3}$

$C^*_{z\,i,n-1,31} = C^*_{I\,i,n-1,12}\hat{z}_{i,n-1,2}\hat{z}_{i,n-1,3} - C^*_{I\,i,n-1,13}\hat{z}^2_{i,n-1,2} - C^*_{I\,i,n-1,22}\hat{z}_{i,n-1,1}\hat{z}_{i,n-1,3} + C^*_{I\,i,n-1,23}\hat{z}_{i,n-1,2}\hat{z}_{i,n-1,1}$

$C^*_{z\,i,n-1,32} = -C^*_{I\,i,n-1,11}\hat{z}_{i,n-1,2}\hat{z}_{i,n-1,3} + C^*_{I\,i,n-1,13}\hat{z}_{i,n-1,1}\hat{z}_{i,n-1,3} + C^*_{I\,i,n-1,21}\hat{z}_{i,n-1,3}\hat{z}_{i,n-1,1} - C^*_{I\,i,n-1,23}\hat{z}^2_{i,n-1,1}$

$C^*_{z\,i,n-1,33} = C^*_{I\,i,n-1,11}\hat{z}_{i,n-1,2}\hat{z}_{i,n-1,3} - C^*_{I\,i,n-1,12}\hat{z}_{i,n-1,1}\hat{z}_{i,n-1,2} - C^*_{I\,i,n-1,21}\hat{z}_{i,n-1,2}\hat{z}_{i,n-1,1} + C^*_{I\,i,n-1,22}\hat{z}^2_{i,n-1,1}$

D.0.3 Dimensionless Connectivity Equation

The discretized connectivity equation is given by

$$\dot{\boldsymbol{r}}_{i,n} - \dot{\boldsymbol{r}}_{i+1,n} + \frac{l}{2}\left(\boldsymbol{\omega}_{i,n}\times\hat{\boldsymbol{z}}_{i,n-1} + \boldsymbol{\omega}_{i+1,n}\times\hat{\boldsymbol{z}}_{i+1,n-1}\right) = \boldsymbol{0} \quad \text{(D.9)}$$

After scaling translational velocities with $r\dot{\gamma}\ [m/s]$, angular velocities with $\dot{\gamma}\ [1/s]$ and length with $r\ [m]$, the dimensionless discretized connectivity equation reads

$$\dot{\boldsymbol{r}}^*_{i,n} - \dot{\boldsymbol{r}}^*_{i+1,n} + r_p(\boldsymbol{\omega}^*_{i,n} \times \hat{\boldsymbol{z}}_{i,n-1} + \boldsymbol{\omega}^*_{i+1,n} \times \hat{\boldsymbol{z}}_{i+1,n-1}) = \mathbf{0} \tag{D.10}$$

where $r_P = l/2r = l/d$ is a fiber segment aspect ratio.

Appendix E

The Physical Pendulum

This appendix gives an overview of the theory of a physical pendulum. The purpose is to provide the basic theoretical support to Chapter 4, which deals with the validation of energy conservation and response time, in the terms of a pendulum period. The physical pendulum is a system composed of a rigid body, which oscillates around an axis that does not pass through its center of mass. A rigid body pivoted from point O is shown in Fig. E.1. The center of mass is at a distance h

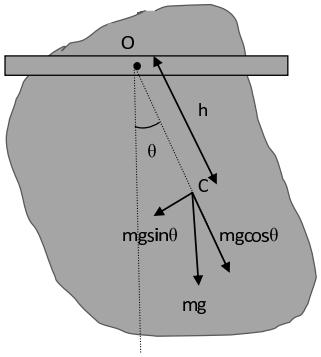

Figure E.1: Physical pendulum

from the point of suspension. The gravity causes a moment around the axis through point O. The moment intensity is $mgh\sin\theta$, where θ is the angle, from the vertical direction, as seen in Fig. E.1. The equation of motion reads

$$I\ddot{\theta} = -mgh\sin(\theta) \tag{E.1}$$

For small angles θ, the approximation $sin(\theta) \approx \theta$ applies and the equation of motion becomes

$$\ddot{\theta} = -\left(\frac{mgh}{I}\right)\theta = -\omega^2\theta \tag{E.2}$$

Since this equation has the same form as a linear harmonic oscillator equation, a physical pendulum motion represents a harmonic oscillation, and the solution is

$$\theta = \theta_{max} cos\left(\omega t + \varphi\right) \tag{E.3}$$

where θ_{max} is a maximum pendulum angular elongation, and the angular frequency is given by

$$\omega = \sqrt{\frac{mgh}{I}} \tag{E.4}$$

Thus, the physical pendulum period is given by

$$T = \frac{2\pi}{\omega} = 2\pi\sqrt{\frac{I}{mgh}} \tag{E.5}$$

A homogeneous rod of lenght l and mass m pivoted from one end is shown in Fig. E.2.

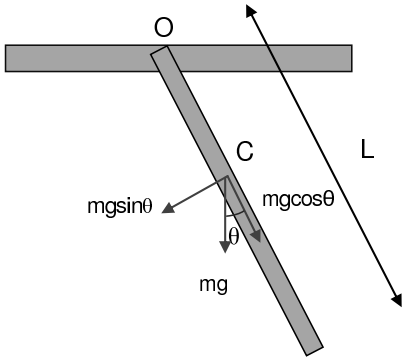

Figure E.2: A homogeneous rod oscillating around end point O

The oscillatory period for the rod reads

$$T = 2\pi\sqrt{\frac{\frac{1}{3}ml^2}{mg\frac{1}{2}}} \tag{E.6}$$

since its moment of inertia is

$$I = \frac{1}{3}ml^2 \tag{E.7}$$